

Are Halo and Galaxy Formation Histories Correlated?

Jeremy L. Tinker¹, Andrew R. Wetzel², and Charlie Conroy³

¹*Center for Cosmology and Particle Physics, Department of Physics, New York University, New York, NY*

²*Department of Astronomy, Yale University, New Haven, CT*

³*Harvard-Smithsonian Center for Astrophysics, Cambridge, MA*

27 July 2011

ABSTRACT

The properties of dark matter halos, including mass growth, correlate with larger scale environment at fixed mass, an effect known as assembly bias. However, whether this environmental dependence manifests itself in galaxy properties remains unclear. We apply a group-finding algorithm to Data Release 7 of the Sloan Digital Sky Survey to estimate the dark matter halo mass of each galaxy and to decompose galaxies into those that exist at the centers of distinct halos and those that orbit as satellites within larger halos. Using the 4000-Å break as a measure of star formation history, we examine the correlation between the quenched fraction of galaxies, f_Q , and large-scale environment, ρ . At all galaxy magnitudes, there is a positive, monotonic relationship between f_Q and ρ . We use the group catalog to decompose this correlation into the contribution from central and satellite galaxies as a function of halo mass. Because satellites are more likely to be quenched than central galaxies, the observed f_Q - ρ correlation is primarily due to variations of the halo mass function with environment, which causes a larger fraction of satellite galaxies at high ρ . For high-mass central galaxies, there is a weak but positive correlation between f_Q and ρ at both fixed galaxy luminosity and fixed halo mass. For low-mass central galaxies ($M_* \lesssim 10^{10.0} M_\odot/h^2$), there is no correlation between f_Q and ρ . The latter results are inconsistent with the strong assembly bias of dark matter halos seen in this mass regime if recent galaxy growth at all correlates with recent halo growth, as we demonstrate through a high-resolution N -body simulation. We also find that the mean stellar age of quenched central galaxies is independent of ρ at fixed M_* , while the formation times of low mass halos vary significantly. We conclude that the processes that halt the star formation of low mass central galaxies are not correlated to the formation histories of their host halos, and old galaxies do not reside preferentially in old halos.

Key words: cosmology: observations—galaxies:clustering—galaxies: groups: general — galaxies: clusters: general — galaxies: evolution

1 INTRODUCTION

Many galaxy properties are correlated with their large- and small-scale environment. The primary examples are the color-density relation and the morphology-density relation (e.g., Oemler 1974; Davis & Geller 1976; Dressler 1980). These results demonstrated that, in the local Universe, galaxies in lower-density regions are typically less massive, and that even at fixed luminosity or mass, they are bluer and more likely to be spirals. With the advent of large-scale galaxy redshift surveys such as the Sloan Digital Sky Survey (SDSS; York et al. 2000), these seminal works have been refined with increased statistical precision (Hogg et al. 2004; Kauffmann et al. 2004; Blanton et al. 2005; Baldry et al. 2006; Park et al. 2007; Bamford et al.

2009) and extended via direct measurements of the correlations between star formation rates and environment (Balogh et al. 2004; Kauffmann et al. 2004) and via measurements out to $z \approx 1$ (Cucciati et al. 2006; Cooper et al. 2007).

Studies that investigated the relative importance of environment on different scales indicated that small-scale environment (Mpc scale) correlates stronger with galaxy properties than large-scale environment (Kauffmann et al. 2004; Blanton et al. 2006; Blanton & Berlind 2007; Wilman et al. 2010). These results suggest that the mass of the dark matter halo in which a galaxy resides plays the dominant role in the galaxy’s formation and evolution. For example, Blanton & Berlind (2007) found that the blue fraction of galaxies in rich groups and clusters is independent of envi-

ronment at fixed halo mass. In this paper we extend these results by focusing on galaxies in low-mass halos.

The definition of environment is thus key to any discussion of this topic. In this paper as in many other works, ‘environment’ is defined as the local *galaxy* density at some smoothing scale. However, the physical interpretation of this definition of environment is not entirely straightforward because galaxy density is a biased measure of dark matter density, in addition to being subject to shot noise and the effects of redshift-space distortions (see, e.g., Cooper et al. 2005). The choice of scale is also important. In this paper we make the distinction between (large-scale) environment and halo mass. We define environment as the local galaxy density on scales larger than the host dark matter halo of a given galaxy, using a fiducial smoothing scale of $10 h^{-1}$ Mpc. Halo mass is similar to ‘small-scale environment’, but the distinction is important. The dispersion of host halo masses for galaxies at a fixed 1 Mpc local density can be 1 dex or more and using distance to the n -th nearest neighbor yields an even larger spread in halo mass (Haas et al. 2011). This scatter demonstrates the need for quantifying halo mass explicitly.

The idea that galaxy properties depend primarily on host halo properties is physically motivated, since the halo virial radius corresponds to a physical transition between infall and virialized motions, capable of supporting strong shock fronts and hot, thermalized gas (e.g., Dekel & Birnboim 2006). In this sense, a galaxy group necessarily corresponds to a single, virialized dark matter halo. This is distinct from many other definitions of ‘group environment’. For example, the ‘Local Group’ is not a group at all in this context, but rather a close pair of separate halos. The difference is an important one: for a halo to enclose both the Milky Way and Andromeda (with one galaxy at the halo center), it would have to be larger than $10^{13} M_{\odot}$ to equal their separation of ~ 800 kpc, a mass at which diffuse halo gas is heated to high temperatures, causing shock heating and stripping of the disks in our galaxy or M31 (or both). As a close pair of $\sim 10^{12} M_{\odot}$ halos, their tidal interactions and gas physics is markedly different: there is no ram pressure and tidal stripping is much weaker. It is thus more informative to quantify halo mass rather than galaxy density on a small scale.

However, environment does play a role in the formation of dark matter halos. In the numerical Universe, dark matter halos exhibit ‘assembly bias’: at fixed mass, halo properties depend on their formation histories (Gao et al. 2005; Harker et al. 2006; Gao & White 2006; Wechsler et al. 2006; Wetzel et al. 2007; Li et al. 2008; Dalal et al. 2008). At low halo mass, older and more concentrated halos form in high density environments. At high mass the effect reverses, with younger, less concentrated halos forming in high-density regions, though the effect is also weaker. Semi-analytic models of galaxy formation predict that this assembly bias propagates into the evolution of galaxies at fixed halo mass, especially in the formation histories and star formation properties of low-luminosity galaxies in low-mass halos (Zhu et al. 2006; Croton et al. 2007). At first glance, these predictions appear in concert with the above observational evidence that the fraction of galaxies (at fixed luminosity) that are red and quenched is highest at high densities.

Another approach to understanding the connection be-

tween galaxies and dark matter is the Halo Occupation Distribution (HOD; see, e.g., Seljak 2000; Peacock & Smith 2000; Scoccimarro et al. 2001; Berlind & Weinberg 2002; Cooray & Sheth 2002). The HOD has emerged as our most powerful tool for understanding the clustering of galaxies and quantifying the bias between galaxies and dark matter, where bias here is defined as the ratio between the galaxy and matter densities on an arbitrary smoothing scale. The central quantity in the HOD is $P(N|M)$, the probability that a halo of mass M contains N galaxies within a defined sample. The galaxy sample may be arbitrarily defined, thus $P(N|M)$ will be different for every sample definition. The bias of galaxies depends strongly on galaxy properties, with strong clustering for galaxies that are brighter, redder, and more elliptical (e.g., Norberg, et al. 2001, 2002; Zehavi et al. 2002; Zehavi, et al. 2005; Zehavi et al. 2010; Li et al. 2006). In the HOD context, these trends are all explained by the different halos that different types of galaxies occupy. Brighter central galaxies live in more massive halos that are more highly clustered. At fixed galaxy mass, redder or more elliptical galaxies are more likely to be satellites in groups or clusters, thus enhancing their clustering. These observations fit into the HOD formalism without any explicit correlation between galaxy formation and environment, other than the fact that massive halos form at high densities (e.g. Bond et al. 1991).

The $P(N|M)$ ansatz has been extended even further in the ‘subhalo abundance matching’ approach, which (in its simplest form) assumes a monotonic relationship between halo mass, M , and galaxy luminosity, L (Kravtsov et al. 2004; Wang et al. 2006; Vale & Ostriker 2006; Conroy et al. 2006; Moster et al. 2010; Conroy & Wechsler 2009; Wetzel & White 2010; Behroozi et al. 2010).¹ Here, if the number density of halos above M is the same as that of galaxies above L , then M halos host galaxies of L brightness. The key to this approach is to include not just isolated halos, but also ‘subhalos’, defined as bound, virialized halos located within the virial radii of larger host halos. The primary assumption of this approach is that (sub)halo mass entirely determines the luminosity of the galaxy within it, regardless of any other properties of the (sub)halo or the galaxy.

The quantity $P(N|M)$ makes the explicit, and strong, assumption that N depends only on M . That is, the properties of galaxies, including luminosity, color, age, and morphology, depend only on the mass of their host dark matter halo and have no additional dependence on a halo’s formation history or environment. This formulation was not proposed with any theoretical prejudice about galaxy formation, but rather it was the simplest implementation and was successful in fitting the clustering properties of nearly all available data. However, the discovery of halo assembly bias, combined with the complex relation between galaxy properties and environment, especially those governing galaxy growth and star formation, calls into question this ansatz.

In Tinker et al. (2008), we sought to test this $P(N|M)$ ansatz through different galaxy clustering measures that probe different environments. We used the two-point cor-

¹ One can use halo maximum circular velocity rather than halo mass, or use galaxy stellar mass rather than galaxy luminosity.

relation function, $\xi_g(r)$, to constrain halo occupation and make predictions for the void probability function. The predictions were in excellent agreement with the measurements, demonstrating the validity of the HOD from high to low densities. Abbas & Sheth (2006) and Skibba et al. (2006) used other galaxy clustering measures to demonstrate that the assumption of $P(N|M)$ is consistent with observed data for luminosity-based galaxy samples. However, Yang et al. (2006) and Wang et al. (2008) found that the clustering of low-mass galaxy groups at fixed mass depends on the color of the galaxies contained within them such that groups with redder galaxies are more highly clustered.

In this paper, we examine the relation between galaxy star formation histories, their host dark matter halos, and their large-scale environment. We explore in particular the extent to which the formation histories of galaxies relate to those of their host halos and whether the assembly bias seen in simulation extends to the galaxy population. We focus on low-mass galaxies, the regime in which halo assembly bias effects are the strongest, and we examine star formation history based on narrow 4000-Å break, D_n4000 , which, unlike color, is insensitive to dust reddening. In order to observationally determine halo masses for SDSS galaxies and separate this from large-scale environment, we construct galaxy group catalogs using the Yang et al. (2005) group-finding algorithm. Our use of a group finder is critical because galaxies of the same properties may occupy halos of a wide range of mass. At fixed stellar mass, galaxies may live at the center of low-mass halos or they may exist as satellites in group or cluster-sized halos. Anywhere between 10-40% of galaxies are satellites, depending on galaxy mass and color (see, e.g., Yang et al. 2008; Zehavi et al. 2010). The distinction between central and satellite galaxies will be the cornerstone of understanding the environmental correlations of galaxy properties.

The evolution of satellite galaxies is more complex, and their properties also depend on position within a halo (e.g., van den Bosch et al. 2008; Hansen et al. 2009; Weinmann et al. 2010). Here we focus on the properties of central galaxies in halos below the group scale. We will explore the observed dependence of satellite star formation rate on galaxy mass, halo mass, and halo-centric radius in detail in a companion paper (Wetzel, Tinker, & Conroy 2011a), hereafter referred to as Paper II. Finally, in a third paper (Wetzel, Tinker, & Conroy 2011b), hereafter referred to as Paper III, we will use these measurements combined with a high-resolution simulation to test various physical mechanisms for the quenching of satellite galaxies.

We examine galaxies selected on either r -band magnitude or stellar mass, M_* , and we examine star formation history based on D_n4000 . Magnitude and D_n4000 have the advantage of being well-defined observationally, though in Paper II we will focus entirely on stellar mass and instantaneous specific star formation rate (SSFR), quantities which are derived and thus more model-dependent, but also more readily physically interpretable. We have examined all halo and environmental trends in both papers selecting on both M_r and M_* as well as examining both D_n4000 and SSFR. While these lead to slight quantitative differences in our results, they do not change any of our results qualitatively.

Throughout, we define a galaxy group as any set of galaxies that occupy a common dark matter halo (includ-

Table 1. Volume-Limited Samples

| M_r | z_{\max} | $N_{\text{gal}}(< M_r)$ | $\log M_*/[h^{-2} M_\odot]$ | $N_{\text{gal}}(> M_*)$ |
|-------|------------|-------------------------|-----------------------------|-------------------------|
| -18.0 | 0.040 | 31729 | 9.4 | 21423 |
| -19.0 | 0.064 | 74987 | 9.8 | 54119 |
| -20.0 | 0.103 | 131658 | 10.2 | 100852 |

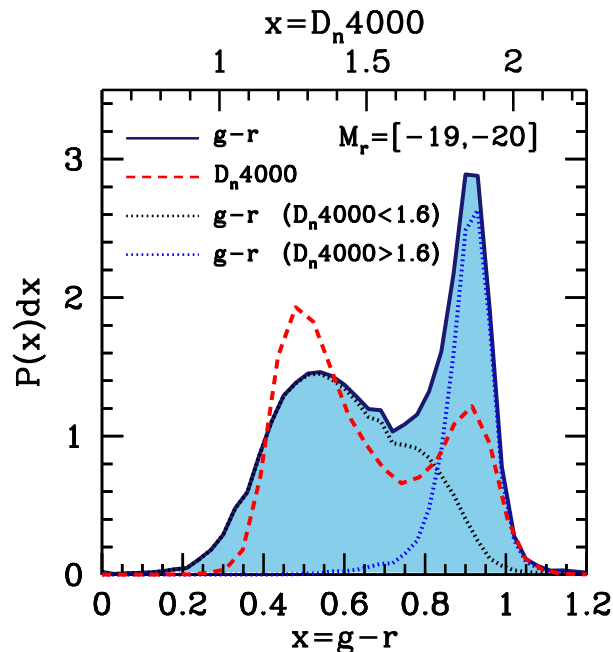


Figure 2. The distribution of $g-r$ color and D_n4000 for $M_r = [-19, -20]$ galaxies. The shaded region shows the distribution of color, with scale on the bottom x -axis. The red dashed curve shows the distribution of D_n4000 for the same galaxies, with scale on the top x -axis. Even though 53% of galaxies are red ($g-r > 0.7$), only 35% of galaxies are truly quenched ($D_n4000 > 1.6$). The blue and black dotted curves show the color distribution for quenched and active galaxies, respectively, according to their D_n4000 values. Quenched galaxies nearly always have red colors, while 23% of active galaxies have red colors, primarily because of dust extinction (e.g., Maller et al. 2009).

ing cluster-mass halos), and we define a halo as having a mean interior density 200 times the background matter density. A *host halo* is a halo that is distinct: its center does not reside within the radius of a larger halo. A *subhalo* is one whose center is located within the radius of a larger halo. For all calculations we assume a flat, Λ CDM cosmology of $(\Omega_m, \sigma_8, \Omega_b, n_s, h_0) = (0.27, 0.82, 0.045, 0.95, 0.7)$. For galaxy magnitudes we do not assume a value of h , but for brevity we write all magnitudes as M_r rather than $M_r - 5 \log h_0$. Stellar masses are in units of M_\odot/h^2 .

2 DATA AND MEASUREMENTS

2.1 NYU Value-Added Galaxy Catalog

To construct our galaxy samples, we use the NYU Value-Added Galaxy Catalog (VAGC; Blanton et al. 2005) based on the spectroscopic sample in Data Release 7 (DR7)

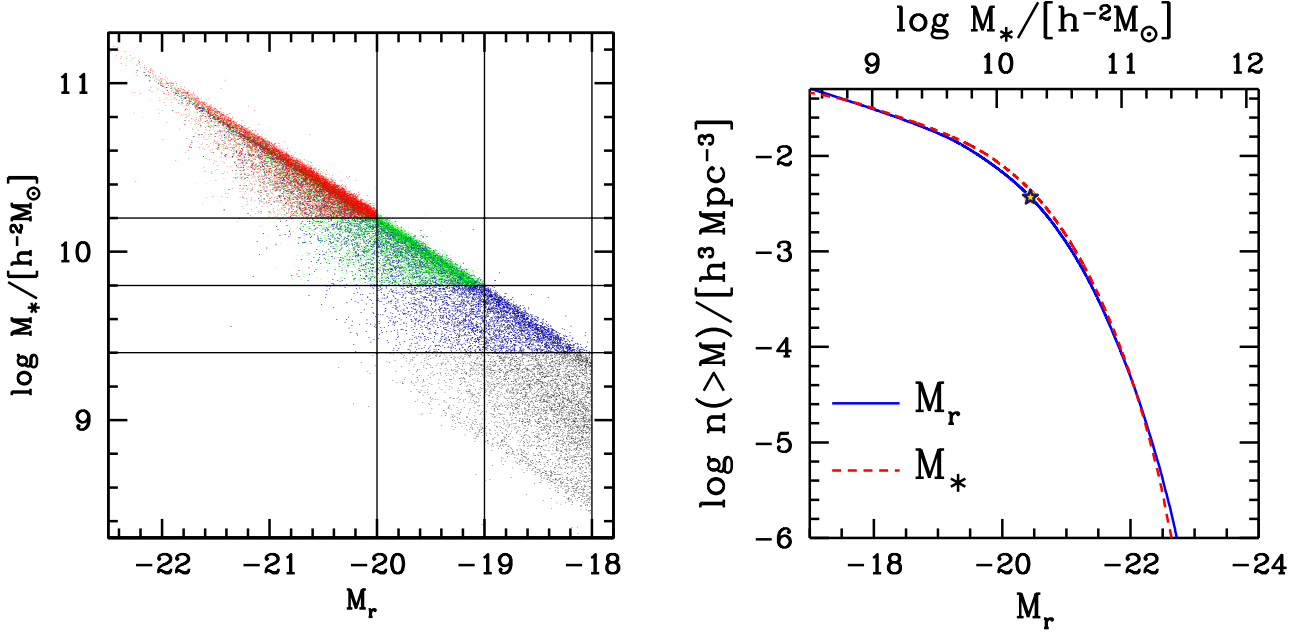


Figure 1. *Left panel:* Relation between r -band magnitude, M_r , and stellar mass, M_* , with the latter taken from the `kcorrect` code of Blanton & Roweis (2007). Vertical lines show the magnitude limits for our volume-limited samples as listed in Table 1, while horizontal lines indicate the stellar mass limits within each volume-limited sample. *Right panel:* Cumulative number density of galaxies as a function of both M_r and M_* , offering a rough conversion between the two. The star indicates M_r^* from the Blanton, et al. (2003) luminosity function.

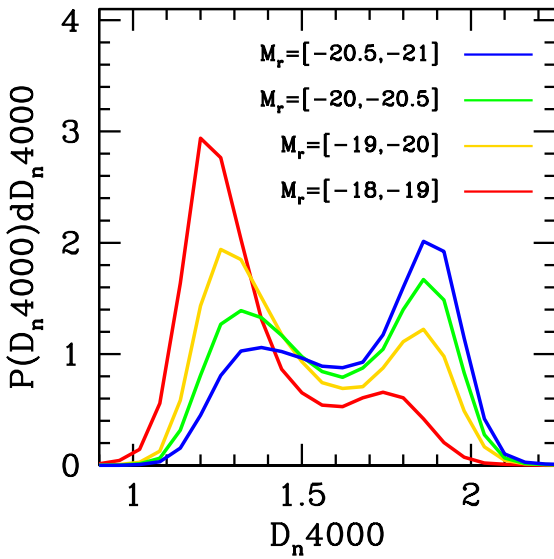


Figure 3. Distribution of D_n4000 values for galaxies in magnitude bins. Faint galaxies are predominantly active while bright galaxies are predominantly quenched but still have a significant active population. All sample distributions are bimodal with a minimum at $D_n4000 \approx 1.6$. We refer to galaxies with $D_n4000 > 1.6$ as ‘quenched’.

of the Sloan Digital Sky Survey (SDSS; Abazajian et al. 2009). Specifically we use `dr72bight34`. We construct three volume-limited samples, as listed in Table 1, which con-

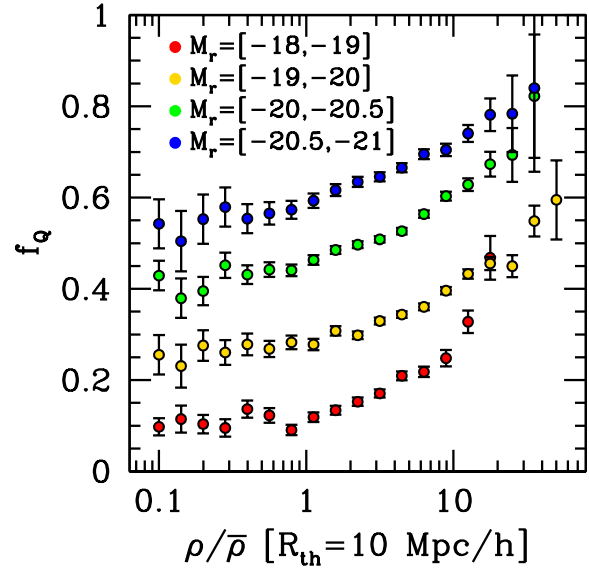


Figure 4. Quenched fraction, f_Q , defined by $D_n4000 > 1.6$, as a function of large-scale ($10 h^{-1} \text{ Mpc}$) density of galaxies. At $\rho/\bar{\rho} > 1$, f_Q rises monotonically with density, while in underdense regions the quenched fraction is nearly constant.

tain all galaxies brighter than $M_r = -18$, $M_r = -19$ and $M_r = -20$, respectively. Within each volume-limited sample, we construct another sample that is complete in stellar mass. The stellar masses are also taken from the VAGC and are derived from the `kcorrect` code of Blanton & Roweis

(2007), which assumes a Chabrier (2003) initial mass function. Fig. 1 (left) shows the comparison between stellar mass and r -band magnitude. The vertical and horizontal lines indicate the magnitude and stellar mass limits, respectively, for our samples. By constructing our stellar mass samples this way, they contain significantly fewer galaxies than the luminosity-defined samples. This limits the statistics and effective halo mass range of the stellar mass samples, but this method has the benefit of requiring no weighting scheme for red galaxies that are fainter than blue galaxies at fixed stellar mass. We will construct groups and present results based upon both sample definitions in order to demonstrate robustness to galaxy property selection. To allow convenient, though approximate, conversion between the two properties, Fig. 1 (right) also shows the cumulative number densities of galaxies based upon M_r and M_* .

For galaxy pairs that are too close to obtain spectra because of the 55 arcsecond width of SDSS fibers ('fiber collisions'), we use the internal correction to the fiber corrections within the VAGC, namely that the collided object is given the redshift of the nearest galaxy in terms of angular separation, provided that this redshift is in agreement with the photometric redshift obtained by with the SDSS photometry (Blanton et al. 2005).

2.2 Bimodality of Galaxy Properties

Galaxies can be roughly divided into two distinct color categories: the 'blue cloud' and the 'red sequence'. The former is comprised of galaxies that are actively forming stars at the current epoch, giving them blue colors. These galaxies are primarily disk-dominated with significant amounts of cool gas. The red sequence is comprised (mostly) of galaxies with old stellar populations, devoid of cold gas, and usually exhibiting elliptical morphology. The bimodality of the galaxy color distribution is well measured at $z = 0$ (Strateva, et al. 2001; Blanton, et al. 2003; Kauffmann et al. 2003; Madgwick et al. 2003) and has been shown to exist at $z = 1$ (Bell et al. 2004; Cooper et al. 2006; Willmer, et al. 2006) and even up to $z = 2$ (Williams et al. 2009).

Using galaxy color as a proxy for star formation activity can be problematic, as dust reddening can cause a gas-rich disk galaxy to be classified as a red sequence object (Maller et al. 2009; Masters et al. 2010). To avoid this problem, we use D_n4000 , which is derived from SDSS spectra. D_n4000 is a diagnostic of the light-weighted age of the stellar population and thus is sensitive to the integrated star formation history of the galaxy. We obtain this quantity from the JHU-MPA spectral reductions² (Brinchmann et al. 2004). Fig. 2 compares the distribution of $g - r$ color to that of D_n4000 for $-19 > M_r > -20$ galaxies, our fiducial magnitude bin throughout this paper. The red sequence is defined a strong peak in the color distribution at $g - r \approx 0.9$ and at $D_n4000 \approx 1.9$. Both distributions are clearly bimodal, but based on color alone one would conclude that the majority of galaxies in this magnitude range are quenched. The picture painted by D_n4000 is strikingly different: the majority of galaxies of this magnitude are instead active, but many

have been dust-reddened. We have confirmed that this population of active but red galaxies is caused primarily by dusty spirals by applying Galaxy Zoo morphological classifications (Lintott et al. 2011) to the sample: $\sim 70\%$ of are identified as spirals, and $\sim 50\%$ are identified as edge-on spirals (see also Masters et al. 2010).

One concern in using galaxy properties defined by spectra is fiber collisions, which cause $\sim 8\%$ of all galaxies in the survey to not have spectra. To correct for this, for each fiber-collided galaxy we draw a random value of D_n4000 based on a sample of spectroscopic galaxies that are within ± 0.25 in M_r and ± 0.05 in $g - r$ of the collided object. This method allows us to use the colors to infer statistically the spectroscopic properties of the collided sample. This method reflects the fact that not all collided red galaxies are truly quenched, and it preserves the fact that the color distribution of collided objects (and the distribution of D_n4000) is distinct from the overall color distribution at the same magnitude. Using this method, our results are generally consistent with those obtained by simply removing the collided galaxies from the samples after constructing the group catalog.

Fig. 3 shows D_n4000 distribution for galaxies of different absolute magnitudes. As seen in previous studies, the bimodal distribution in sub- L_* galaxies is apparent but is dominated by a younger, active population. At $L \gtrsim L_*$, the bimodality is still present but has been tilted to the older, quenched population. The brightest galaxies are dominated by an red, old population that is not forming stars at any appreciable rate. Because the minimum of the bimodality occurs at $D_n4000 = 1.6$ across all magnitudes we explore, we define galaxies with $D_n4000 < 1.6$ as 'active' and $D_n4000 > 1.6$ as 'quenched'.

Another possible concern with galaxy properties defined by SDSS spectra is the finite 3 arcsec aperture of the fibers, corresponding to $\sim 2 h^{-1}$ kpc at the redshifts we consider. Thus, for many galaxies the SDSS fiber covers only the inner light profile, where the stellar population may be older (or younger) than the rest of the galaxy. As can be seen in Fig. 3, the fraction of blue galaxies that are labeled as quenched via D_n4000 is negligible compared to the fraction of red galaxies that have active stellar populations. Thus, while aperture effects may bias D_n4000 values somewhat, the effect of dust obscuration on color is far more important.

2.3 Measuring Large-scale Environment

For each galaxy, we determine the large-scale environment by counting the number of neighboring galaxies within a sphere of radius $10 h^{-1}$ Mpc centered on each galaxy. This quantity is a biased indicator of the dark matter density field, but at $10 h^{-1}$ Mpc this bias is a simple linear factor and any stochasticity is minimal. We count the number of galaxies above the corresponding magnitude threshold for the each sample, and so the tracer of the density field has a different bias for each sample. We do not correct for this between the samples, but note that the relative bias between $M_r < -18$, -19 , and -20 samples is at the $\sim 5\%$ level (Swanson et al. 2008). This galaxy density measurement is affected by galaxy peculiar velocities, but this effect is minimal at $10 h^{-1}$ Mpc, as we demonstrate in Appendix A.

We also choose $10 h^{-1}$ Mpc as it represents a clear distinction from a galaxy's small-scale environment as encapsu-

² <http://www.mpa-garching.mpg.de/SDSS/DR7/>

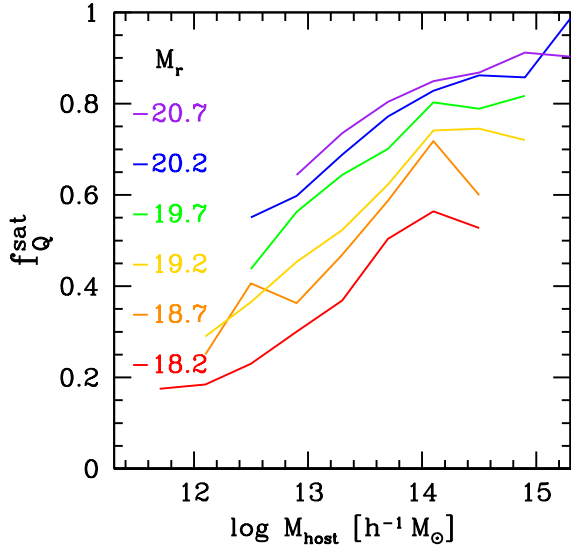


Figure 5. Quenched fraction of satellite galaxies, f_Q^{sat} , as a function of M_{host} for bins in galaxy magnitude. At fixed halo mass, brighter satellites are more likely to be quenched, and satellites of all magnitudes show a similar increase in quenched fraction with halo mass.

lated by its host halo, especially since $10 h^{-1} \text{ Mpc}$ represents the maximum extent from which the most massive galaxy clusters have accreted their mass. In tests we find that our results show little dependence on the exact smoothing scale chosen. In Paper II we will further discuss the properties of galaxies on the outskirts of groups and clusters.

To correct for survey geometry and incompleteness, we use of random catalogs. For each volume-limited sample, we produce a catalog of 10^7 random points distributed with the angular selection function of SDSS DR7 using the angular mask provided with the VAGC in combination with the software package *mangle* (Swanson et al. 2008). Each random point is also assigned a random redshift such that the comoving space density of randoms is constant with redshift. For each galaxy, we correct for incompleteness by multiplying the observed number of galaxies by the ratio of the number of random points divided by the expected number of randoms if the completeness were unity. The large number of random points ensures that shot noise within each $10 h^{-1} \text{ Mpc}$ sphere is at the sub-percent level.

Fig. 4 shows the fraction of quenched galaxies as a function of large-scale density. For all magnitude bins there is clear dependence on density such that quenched galaxies preferentially live in overdense environments. At $\rho/\bar{\rho} > 1$, the slope of the quenched fraction with $\log \rho/\bar{\rho}$ is roughly independent of galaxy magnitude. At $\rho/\bar{\rho} > 10$, the fraction of quenched galaxies in the faintest magnitude bin rises steeply. Other studies have also noted that the faintest red galaxies predominantly are found in the highest density regions (Hogg et al. 2004; Blanton et al. 2005).

3 GROUP FINDING ALGORITHM

Motivated by the framework of the HOD model, we assign halos to galaxies using the group-finding algorithm detailed in Yang et al. (2005) and applied to the SDSS in a series of papers (Yang et al. 2007, 2008, 2009; Weinmann et al. 2006; Wang et al. 2008; van den Bosch et al. 2008). Given the known statistics of dark matter halos, the halo masses of groups of galaxies can be retrofitted to the observed distribution of galaxies. Because this algorithm has been described in detail in the papers above, in this section we give a synopsis of the group finder and the minor modifications we made to the algorithm, and we provide a more thorough description in Appendix B.

Our starting point differs from the algorithm of Yang et al. (2005). To begin, we ascribe to each galaxy in the VAGC a dark matter halo mass via the subhalo abundance matching method described in §1. Typically, abundance matching is used to put galaxies into a population of dark matter (sub)halos, but we invert this process to put (sub)halos around *galaxies* as the first step in the group-finding algorithm. The abundance matching method relates galaxy luminosity (or stellar mass) to (sub)halo mass by assuming that the two are monotonically related. Thus, a (sub)halo of mass M_0 contains a galaxy of luminosity L_0 such that

$$\int_{L_0}^{\infty} \Phi(L) dL = \int_{M_0}^{\infty} n_{\text{tot}}(M) dM \quad (1)$$

where $\Phi(L)$ is the galaxy luminosity function (or alternately the stellar mass function) and $n_{\text{tot}}(M)$ is the halo plus subhalo mass function.

In applying equation (1) we use the Tinker et al. (2008) function for the halo mass function and the subhalo mass function in Tinker & Wetzel (2010) (their equation 12; but we have changed the normalization from 0.3 to 0.2 to account for the differences in the subhalo mass function between redshift 1 and 0). The total number density of halos of mass M is then

$$n_{\text{tot}}(M) = n(M_{\text{host}}) + \int n(M_{\text{sub}}|M_{\text{host}})n(M_{\text{host}}) dM_{\text{host}} \quad (2)$$

where we have denoted halos that are distinct as ‘host’ halos and halos that are contained within host halos as ‘sub’. Thus, each galaxy is given a halo mass regardless of whether it is a satellite within a larger host halo or resides in the field³.

To obtain the left-hand side of equation (1), we sum all galaxies, L_i , brighter than L_0 , weighed by V_{max} to obtain the number density, given by,

$$n(> L_0) = \sum_{L_i > L_0} V_{\text{max}}^{-1}(L_i) \quad (3)$$

where V_{max} is the maximum volume to which each galaxy is observed, as calculated in the VAGC to account for survey incompleteness. Once again, luminosity can be replaced by stellar mass, and a comparison of the cumulative density of galaxies as a function of magnitude and M_* is given

³ Note that M_{sub} is the mass of the subhalo at the time of accretion. See details in Tinker & Wetzel (2010) and a discussion of subhalo finding in Paper III.

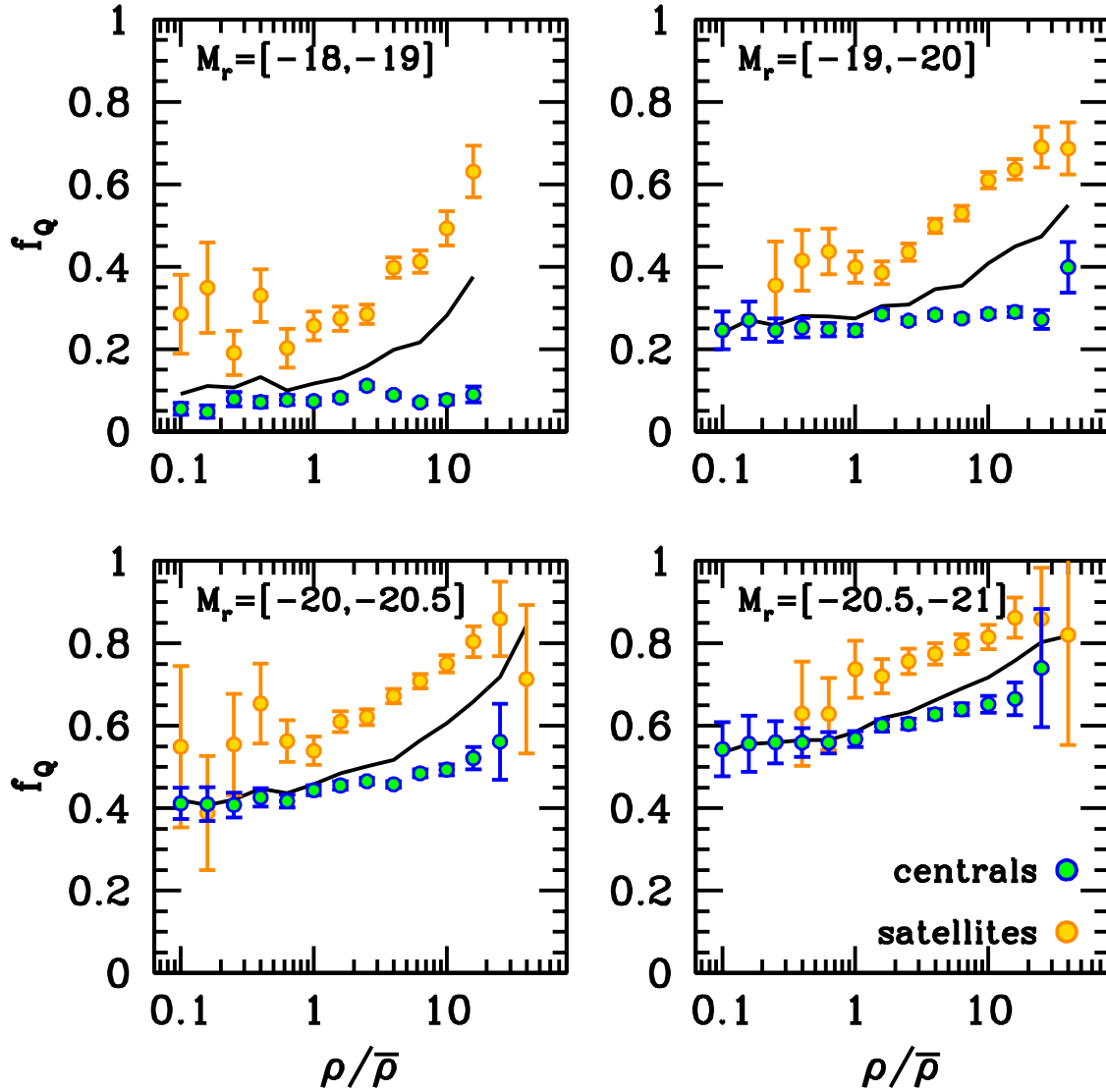


Figure 6. Quenched fraction, f_Q , vs. $10 h^{-1}$ Mpc overdensity, $\rho/\bar{\rho}$, for various bins in galaxy magnitude. In each panel, the solid curve is the overall f_Q - $\rho/\bar{\rho}$ relation, with the filled circles showing f_Q^{cen} and f_Q^{sat} . Bright central galaxies do show a slight increase in quenched fraction with density.

in Fig. 1. Although we later cull the VAGC to create the volume-limited samples in Table 1, using the full flux-limited catalog suppresses sample variance in the calculation of the luminosity function for the initial halo mass assignment.

In the Yang et al. (2005) methodology, this initial matching of galaxies to groups and halo mass is done with a redshift-space friends-of-friends (FOF) linking algorithm (see also Berlind, et al. 2006). Using the inverse abundance matching approach, we find results that are consistent with the FOF algorithm. See the tests in Appendix C.

Once a halo has been assigned to each galaxy, each galaxy has an associated halo mass, virial radius, and velocity dispersion via the virial theorem. We then determine the probability that each galaxy is a central galaxy in a host halo or a satellite galaxy in a subhalo. If, projected

on the sky, a galaxy lies within a more massive galaxy's virial radius, we determine an angular probability that the galaxy is a satellite by assuming that the number density profile of satellite galaxies follows the dark matter given by an NFW (Navarro et al. 1997b) profile. We assume the concentration-mass relation given by Macciò et al. (2008) for our cosmology, but note that the results are insensitive to this choice. We also assign a line-of-sight satellite probability to the galaxy given its redshift offset from the more massive galaxy, where we assume that the host halo's satellites are distributed in a Gaussian along the line of sight. If the product of the angular and line-of-sight probability is above a calibrated constant, then the galaxy is considered to be a satellite in the larger host halo. Once we have applied this routine to all galaxies and we have a list of candidate

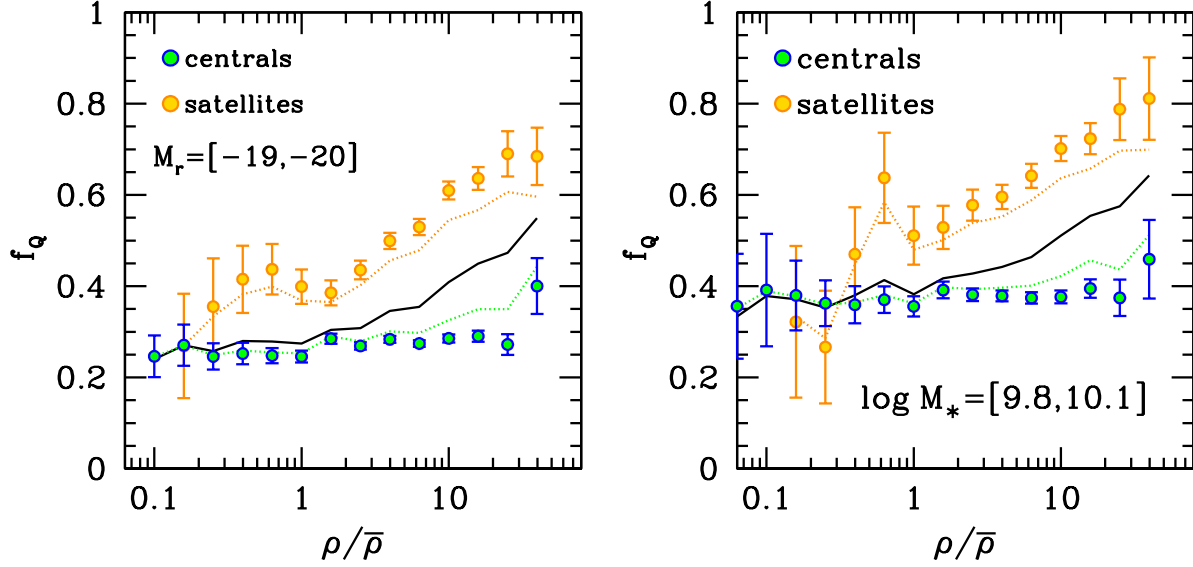


Figure 7. *Left panel:* The relation between quenched fraction, f_Q , and 10 h^{-1} Mpc overdensity, $\rho/\bar{\rho}$, for $M_r = [-19, -20]$ galaxies. The solid curve shows the overall relation from Fig. 4. The different filled circles show the quenched fraction divided into central and satellite galaxies. The dotted curves show the measurements without correcting for satellite-central misclassification in the group finder (this correction is described in detail in Appendix C). *Right panel:* Same as left panel, but using the galaxy group catalog defined with stellar mass as opposed to galaxy luminosity as the tracer of group mass. The number density of galaxies with $M_* > 10^{9.8} M_\odot/h^2$ is $\sim 30\%$ lower than that of galaxies with $M_r < -19$ (see Fig. 1), thus the central galaxies in the right hand panel occupy slightly higher mass halos.

host halos, we recompute host halo masses, again by the abundance matching method. However, from this point on, we assume instead that host halo mass correlates with the *total* luminosity of the group. Thus, we use the halo mass function in equation (1) for host halos only (no subhalos), and the luminosity now is the *total* luminosity of the galaxies within the halo. We iterate this procedure until host halo masses for the groups have converged. Our catalog contains groups varying in mass from 2×10^{11} to $10^{15} h^{-1} M_\odot$.

For each sample, we perform the group-finding procedure once using total galaxy luminosity as the tracer of halo mass and once using stellar mass as the tracer of halo mass. There is evidence that stellar mass correlates stronger with halo mass than luminosity, especially when dividing a galaxy sample by color (Mandelbaum et al. 2006; More et al. 2010). However, there are also significant uncertainties in determining stellar mass from broadband optical magnitudes (e.g., Conroy et al. 2009; Conroy & Gunn 2010), and so it is not clear whether stellar mass or luminosity is preferable here. Nonetheless, we will demonstrate that all our conclusions are robust to choice of halo mass tracer.

Note that our algorithm defines the brightest (or most massive) group galaxy as the central galaxy, that is, the galaxy residing at the minimum of the host halo’s potential well. For halos with $M_{\text{host}} \lesssim 10^{13} h^{-1} M_\odot$, central galaxies are expected to be the brightest galaxy in the halo the vast majority of the time (Zehavi, et al. 2005; Tinker et al. 2005; Zheng et al. 2005; Yang et al. 2009). For cluster-sized halos, $M_{\text{host}} \gtrsim 10^{14} h^{-1} M_\odot$, whether the brightest galaxy is always central galaxy is not clear (Skibba et al. 2011). In statistical terms, halos of this mass are rare and do not contribute significantly to the results presented here. Because

we focus on central galaxies with $L \lesssim L_*$ luminosities, this is not a concern for our results.

Yang et al. (2005) and subsequent papers have demonstrated the efficacy of the halo-based group finder, but the approach is not infallible. The algorithm is designed to obtain the correct mean number of galaxies per halo, but because of projection effects and redshift-space distortions, some galaxies will erroneously be labeled as ‘central’ when in fact they are within the virial radius of a larger halo, while other central galaxies will falsely be labeled as ‘satellites’. This misclassification of galaxy type means that the measured fraction of central and satellite galaxies that are quenched will be biased because satellite galaxies are more likely to be quenched than central galaxies at fixed M_* . In Appendix C we use a high-resolution N -body simulation to quantify the false-classification rate and demonstrate how to statistically correct the measurements of f_Q for this effect. On average, $\sim 10\%$ of galaxies are misclassified, and all of the results in this paper include a correction for this misclassification, except where stated otherwise. We note that the group-finding algorithm is actually *more* efficient at identifying the central galaxies than satellite galaxies within a given sample, yielding a completeness of $\sim 95\%$ for most central galaxies (see App. C).

We have also checked our results against a SDSS DR7 version of the Yang et al. (2007) group catalog (kindly supplied by Frank van den Bosch), incorporating the same `kcorrect` stellar masses D_n4000 measurements we use here but retaining differences in assumed cosmology, halo virial definitions, and group-making methodology. All of the results are consistent within errors, demonstrating the robust-

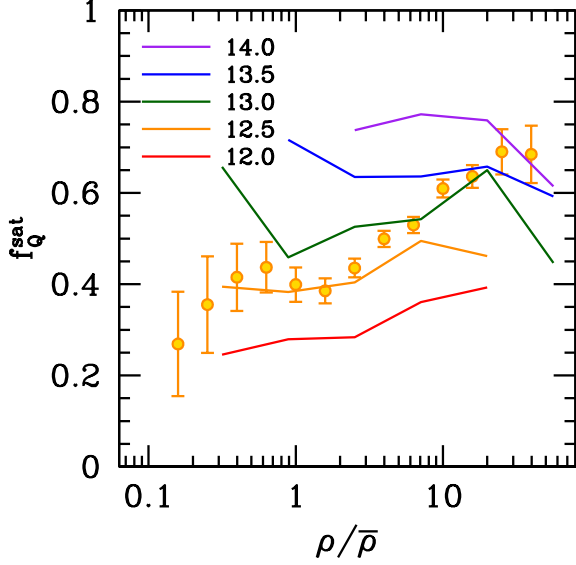


Figure 8. Quenched fraction of satellites, f_Q^{sat} , as a function of $10 h^{-1}$ Mpc overdensity, $\rho/\bar{\rho}$, for satellites with $M_r = [-19, -20]$. Filled circles show the measurements from Fig. 7. Solid curves show f_Q^{sat} in bins of $\log M_{\text{host}}$.

ness of the iterative group-making method to the details of the initialization of the procedure.

4 RESULTS

4.1 Properties of Satellite Galaxies at Fixed Halo Mass

For our fiducial results we examine a bin in magnitude of $M_r = [-19, -20]$. These galaxies are faint enough that they span a wide range of host halo masses (as satellite galaxies) but bright enough that a volume-limited sample contains sufficient statistics for fine binning in halo mass. By looking at galaxies in a relatively narrow range of luminosities, we are restricting our analysis to galaxies that are in a narrow range of M_{sub} (for satellite galaxies) and M_{host} (for central galaxies).

Fig. 5 shows the fraction of quenched satellites, f_Q^{sat} , as a function of M_{host} for bins in M_r . The slope of f_Q^{sat} is independent of galaxy magnitude, but the amplitude increases monotonically with M_r . These results indicate that accretion of a galaxy onto a larger halo contributes significantly to the buildup of quenched, passive galaxies, in agreement with previous works (e.g., van den Bosch et al. 2008; Tinker & Wetzel 2010).

The satellite trends in Fig. 5 are broadly consistent with previous results on galaxy mass and halo mass dependence. Using the maxBCG cluster sample, Hansen et al. (2009) found that the red fraction of galaxies increases with cluster richness, though their red fraction is somewhat higher than our quenched fraction due to the use of color rather than a dust-insensitive diagnostic. Other works using more direct star formation rate indicators have found more similar trends (Weinmann et al. 2006; Kimm et al. 2009;

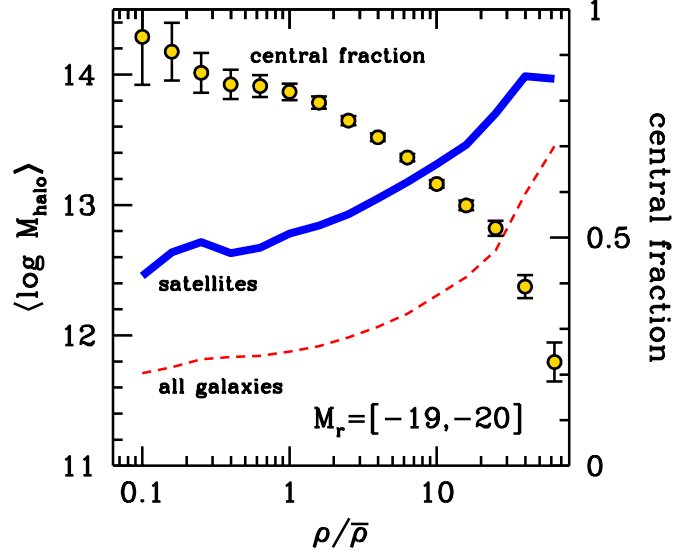


Figure 9. Solid and dashed curves indicate the mean $\log M_{\text{host}}$ as a function of $10 h^{-1}$ Mpc overdensity, $\rho/\bar{\rho}$, for satellite galaxies and all galaxies in the $M_r = [-19, -20]$ bin, respectively. Here, $\langle \log M_{\text{host}} \rangle$ is a galaxy-number weighted mean. Unlike central galaxies, the typical halo mass probed by satellite galaxies increases with density. The filled circles indicate the fraction of all galaxies that are central galaxies as a function of $\rho/\bar{\rho}$, as given by the right-hand y -axis.

Weinmann et al. 2010; von der Linden et al. 2010). We will examine trends of satellite quenching in much more detail in Papers II and III. For now, these results will be important when interpreting the correlations with density in Fig. 4.

4.2 Dissecting the Correlations with Density

Fig. 6 shows the f_Q - $\rho/\bar{\rho}$ relation, broken into central and satellite galaxies, for four magnitude bins. For $L \lesssim L_*$ galaxies, the quenched fraction of central galaxies is independent of large-scale density, spanning the entire range of environments from the deepest voids ($\rho/\bar{\rho} \sim 0.1$) to cluster infall regions ($\rho/\bar{\rho} \gtrsim 10$). The entire correlation with environment is driven by the satellite galaxies. The results are consistent with the scenario in which all environmental correlations are due to the change in the halo mass function. However, for the $M_r = [-20.5, -21]$ magnitude bin there is a clear dependence of f_Q^{cen} with density, increasing from $f_Q = 0.55$ to 0.65 over two decades in density. We will discuss the brighter galaxies subsequently, focusing now on understanding the $f_Q - \rho/\bar{\rho}$ correlation for our fiducial sample.

The left panel in Fig. 7 shows the f_Q - $\rho/\bar{\rho}$ relation for $M_r = [-19, -20]$ galaxies taken from Fig. 6b. The dotted curves indicate the raw quenched fractions, uncorrected for satellite-central mislabeling. Because mislabeling only increases f_Q^{cen} and decreases f_Q^{sat} , these curves can be considered upper and lower limits on these two quantities, respectively. The right panel shows the same breakdown for groups defined by stellar mass rather than luminosity. In both panels, the dependence of f_Q on environment is caused entirely satellite galaxies; f_Q^{sat} rises rapidly when $\rho/\bar{\rho} > 1$.

Understanding this satellite dependence on $\rho/\bar{\rho}$ requires a decomposition into host halo mass. As was demonstrated in Fig. 5, the quenched fraction of satellite galaxies at fixed luminosity is a strong function of M_{host} . Fig. 8 breaks $f_{\text{Q}}^{\text{sat}}$ into bins of fixed M_{host} . When controlling for halo mass, the quenched fraction of satellites also is independent of environment within the statistics of the sample. Thus, the observed correlation between f_{Q} and $\rho/\bar{\rho}$ simply arises from the change in the halo mass function with environment.

Fig. 9 shows the relative number of centrals and satellites as a function of large-scale environment. Unsurprisingly, central galaxies dominate the statistics in the voids. As $\rho/\bar{\rho}$ increases, the central fraction monotonically decreases, dropping under 50% at $\rho/\bar{\rho} > 20$. Because we are looking at a bin in galaxy magnitude, the halo mass probed by centrals is constant with density at $\log M \sim 11.7$, but the typical halo mass probed by satellite galaxies monotonically increases with density. At 10 times the mean galaxy density, $\langle \log M_{\text{host}} \rangle \sim 13$ for satellite galaxies.

The change in $\langle \log M_{\text{host}} \rangle$ with large-scale density is a well-understood phenomenon: more massive dark matter halos are more likely form in higher overdensities (e.g., Bond et al. 1991; Sheth & Tormen 2002). Fig. 5 demonstrates that f_{Q} depends on M_{host} , thus as ρ increases the quenched fraction of satellites increases as a result of the changing halo mass function.

4.3 Bright Central Galaxies

As demonstrated in Fig. 6, the quenched fraction of $L > L_*$ central galaxies does exhibit a weak but significant correlation with density. Using our Poisson error bars, a line with slope $d f_{\text{Q}}^{\text{sat}} / d \log \rho = 0.08$ yields a $\Delta\chi^2$ of 25 relative to the best-fit constant value. Due to scatter between M_r and M_{halo} , central galaxies in this magnitude bin span a range in halo mass. Thus we must determine if this correlation is due to an intrinsic relationship between f_{Q} and density or a change in the typical halo mass probed in low and high densities. Fig. 10 shows the results for the $M_r = [-20.5, -21]$ central galaxies broken into bins of fixed halo mass. For each halo mass bin, the quenched fraction shows a correlation with density comparable to that of the overall magnitude bin, which demonstrates that more massive galaxies exhibit a true correlation with environment at fixed halo mass.

5 CONFRONTING THEORY WITH OBSERVATIONS

5.1 Quenched Galaxy Fractions vs. Old Halo Fractions

Although a full model of galaxy formation requires incorporation of many unsolved physical processes, it is possible to test the ansatz that the oldest (or slowest growing) galaxies reside in the oldest halos. In the context of the observational metric used here, ‘old’ galaxies have ceased growing in mass through star formation⁴, while ‘old’ halos have accumulated

⁴ Low-mass, quenched galaxies may increase their mass through merging, but significant mass growth through mergers is unlikely for sub- L_* galaxies (Maller 2008; Conroy & Wechsler 2009) and

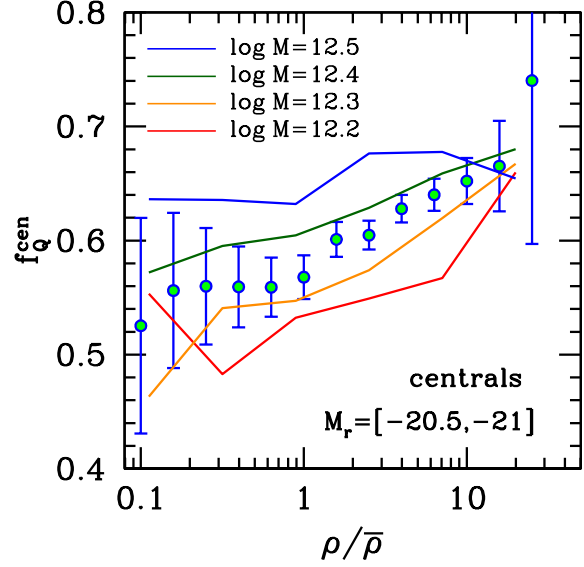


Figure 10. Quenched fraction of bright central galaxies vs. $10 h^{-1} \text{Mpc}$ overdensity. The circles represent $f_{\text{Q}}^{\text{cen}}$ for all central galaxies in this magnitude bin, while the curves show these galaxies split into different halo masses, demonstrating that the increase in quenched fraction with density also persists for fixed halo mass.

most of their mass at early times and have little present mass growth.

In this section we compare theoretical predictions to results from the group catalog that uses stellar mass rather than luminosity to estimate halo mass. We create predictions using halos in a high-resolution N -body simulation described in Appendix C and Paper III. This simulation has sufficient mass and spatial resolution to track the evolution of halos and subhalos down to $10^{11} h^{-1} M_{\odot}$. We populate the halos and subhalos of this simulation with galaxies using the abundance matching technique described in §2, assigning galaxy luminosities with the Blanton, et al. (2003) luminosity function. This allows us to calculate $\rho/\bar{\rho}$ for objects in the simulation in the same manner as our DR7 results⁵.

Fig. 11 shows $f_{\text{Q}}-\rho/\bar{\rho}$ for three bins in galaxy mass (all less massive than the knee in the stellar mass function). In each stellar mass bin, the quenched fraction is independent of environment, consistent with the results from §4. From the group catalog, these galaxies live in halos of mass $\log M_{\text{host}} = 11.4, 11.5$, and 11.6 . We bin the halos in the simulation to match the halo masses probed in the stellar mass samples in Fig. 11. In each bin, the halos are divided into ‘old’ and ‘young’ using the fractional growth rate of each halo. In each panel, we plot the old fraction of halos, f_{old} , as a function of $\rho/\bar{\rho}$, normalized such that the overall old fraction of halos in each mass bin is the same as $f_{\text{Q}}^{\text{cen}}$ of

major mergers would more likely involve a gas-rich galaxy, leading to significant star formation.

⁵ When measuring ρ for galaxies in the stellar mass limited group sample, we use the full volume-limited galaxy sample (to the magnitude limit of the volume) in order to maximize the statistics with which we measure density.

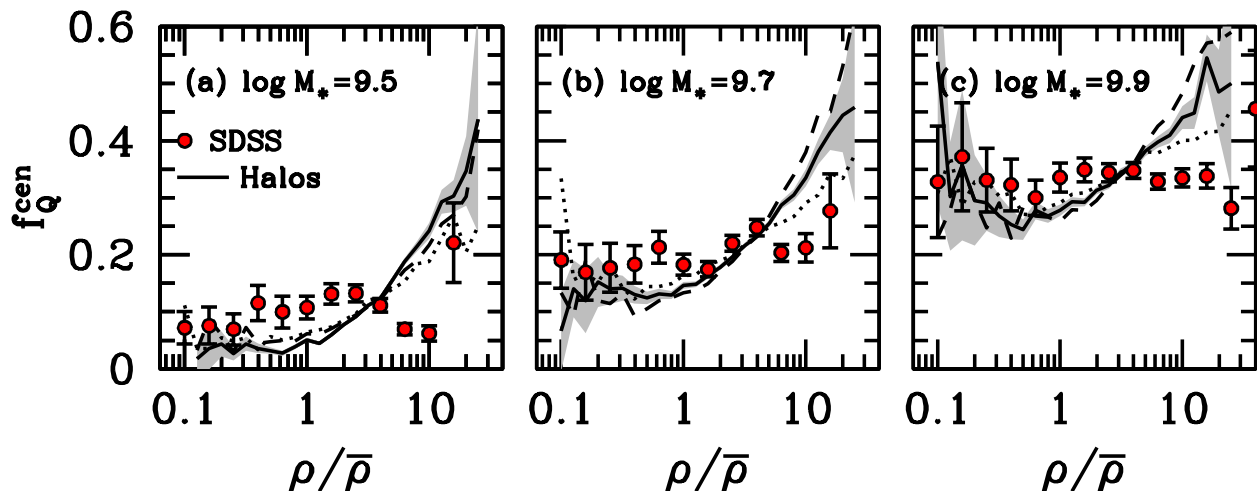


Figure 11. Central quenched fraction, f_Q^{cen} vs. $10 h^{-1}$ Mpc overdensity, $\rho/\bar{\rho}$, in three bins of stellar mass. Filled circles indicate the measurements from the group catalog. The mean logarithmic halo mass for each stellar mass bin is 11.4, 11.5 and 11.6 for panels (a), (b), and (c), respectively. Curves indicate the ‘old’ fraction of dark matter halos in the corresponding mass ranges, where ‘old halos’ are defined as those with the lowest growth since a given redshift, and the growth threshold is chosen to match the corresponding fraction of quenched central galaxies. The solid curves show halos with lowest growth from $z = 0.5$ to $z = 0$, while the dotted and dashed curves are from $z = 1.0$ and $z = 0.3$, respectively. For halos, $\rho/\bar{\rho}$ is measured in the same manner as the data, using galaxy density on the $10 h^{-1}$ Mpc scale. Galaxies are placed into halos and subhalos using Eq. (1). All errors are Poisson. Galaxies with the lowest growth rates do not simply reside in halos with lowest growth rates.

the galaxies. In each panel, the f_{old} depends strongly on $\rho/\bar{\rho}$ such that older halos are preferentially found in high-density environments. This is consistent with earlier numerical results on assembly bias in which old, low-mass halos are more highly clustered than young halos of the same mass (see the references in §1). The different curves in each panel represent different redshift baselines over which to calculate the halo growth rate, defined⁶ as $1 - M(z)/M(0)$, where $z = 0.3$, 0.5 , and 1.0 . Using a shorter redshift baselines leads to a somewhat stronger environmental dependence. But regardless of the definition of halo growth rate, the trend for the halos is not matched by the galaxies. This implies that halo formation history is not correlated with galaxy formation history; at fixed stellar mass, old, quenched galaxies and young, star-forming galaxies live in halos drawn effectively randomly from the distribution of halo growth rates.

To demonstrate this result more clearly, Fig. 12 shows the ratio of the quenched fractions in high- and low-density regions as a function of central galaxy stellar mass. The ratio for SDSS centrals is near unity at all M_* . For galaxies $\log M_* \lesssim 10$, the results are inconsistent with halo growth being correlated with galaxy growth.

⁶ Note that the halo mass used, $M(z)$, is the *maximum* mass the halo has achieved up to redshift z . The maximal mass should correlate closer to galaxy stellar mass than instantaneous mass (Wetzel & White 2010). Halos that lose mass from redshift z to zero would then have growth rates of 0. The rank-ordering of halos by growth rate is insensitive to choice of instantaneous versus maximum mass.

5.2 Halo Formation Times Versus the Redshift of Galaxy Quenching

Rather than assuming a monotonic relationship between galaxy age and halo age, we can also test whether halo formation times correlate with inferred galaxy quenching times for central galaxies. We define quenching time as the look-back time to the redshift at which a galaxy last formed stars. This comparison is model-dependent, both on the observational and theoretical sides, but we will use quantities and parameters to maximize the validity of the comparison.

To model quenched galaxies with stellar population synthesis (SPS) models, we assume a single burst of star formation. Using the SPS models of Conroy et al. (2009) and Conroy & Gunn (2010) we calculate the time evolution of D_n4000 . For these calculations, we assume an initial mass function of Chabrier (2003) and solar metallicity. To model actively star forming galaxies, we assume a star formation history of $SFR \propto t \times \exp(-t/\tau)$ where $\tau = 3.5$ Gyr, consistent with the results of Noeske et al. (2007) for the stellar masses probed here (see Paper III for full details regarding the determination of τ). Once again, we assume solar metallicity in order to calculate D_n4000 as a function time. With these models, we create a lookup table to determine either the quenching timescale or formation timescale for passive and active galaxies, respectively. These timescales are model dependent, being especially sensitive to the metallicity assumed. Thus, the quantity we compare to theoretical predictions is the variation relative to the mean timescale as a function of density. This quantity removes a significant portion of the model dependence.

For dark matter halos, a common quantity used to measure the formation time of a halo is $t_{1/2}$ the time since a halo

accumulated half its current mass. However, for this measure the peak in the age distribution is ~ 9.5 Gyr ($z \sim 1.6$). Most low-mass quenched galaxies have migrated to the red sequence at $z < 1$ (Drory et al. 2009), demanding a measure of halo formation time that probes more recent structure formation. To this end, we use t_{85} the time (in Gyr) since a halo reached 85% of its maximal mass. For this measure, the peak in the halo age distribution is ~ 4 Gyr ($z \sim 0.4$), but with a broad tail to higher redshift.

Fig. 13a shows the mean D_n4000 values as a function of $\rho/\bar{\rho}$ for low-mass quenched central galaxies ($D_n4000 > 1.6$). The mean D_n4000 does not vary with density, implying that the quenching time is constant with density as well. The mean quenching timescale is constant to within ~ 100 Myr across all densities. Fig. 13b compares these results to the formation times of dark matter halos. The solid curve is the change in t_{85} relative to the mean for all halos with $\log M_{\text{halo}} = 11.5 \pm 0.15$ (equivalent to the host halo masses for galaxies with $M_* = 10^{9.7} M_\odot/h^2$). In this comparison, the key assumption is not that the oldest halos contain quenched galaxies, but rather that the quenching time correlates with halo formation epoch. Under this assumption, the mean quenching timescale should vary by roughly 1.3 Gyr with density. If we combine these two assumptions we obtain the dashed curve—here, we isolate the oldest 20% of galaxies in each bin in ρ and determine Δt_{85} for only these halos. In this scenario, the mean formation time varies by nearly 3 Gyr from low to high densities.

The dotted curve plots $\Delta t_{1/2}$ rather than using t_{85} , which shows no correlation with density. However, as we argue above, using a timescale that probes structure at $z > 1$ is unlikely to have any correlation with the recent star formation and growth of galaxies, in contrast to our chosen statistic of t_{85} . Recent halo growth correlates strongly with current environment, but if one measures halo growth so far in the past, these correlations become washed out unless one probes the wings of the distribution.

Fig. 13c is parallel to 13a, but now for star-forming central galaxies ($D_n4000 < 1.6$). Once again, the mean D_n4000 is nearly independent of density. When converting to formation timescale, however, a slight positive trend with ρ is apparent; the timescale varies by roughly 0.6 Gyr from low to high densities. Results for dark matter halos show a stronger trend with density, especially at $\rho/\bar{\rho} \gtrsim 10$. Under the assumptions of our stellar population synthesis models, star forming galaxies in high densities are slightly older than their counterparts in underdensities, but the amplitude of the effect is about half what one would predict using the formation times of dark matter halos.

5.3 Evolution of the Stellar-to-Halo Mass Ratio

Figs. 11 and 13 imply that halo growth rates are not correlated with galaxy growth rates for galaxies below the knee in the stellar mass function—or, perhaps more straightforwardly, that the mechanisms the quench galaxy star formation are not correlated with dark matter growth. If halo growth rate is indeed uncorrelated with galaxy growth rate, then the M_*/M_{halo} ratio for low-mass galaxies will evolve differently for central quenched galaxies as compared with those that remain active. For quenched galaxies, M_* is essentially fixed while M_{halo} continues to evolve, while ac-

tive galaxies continue to grow at a much higher fractional rate than their halos (see, e.g., Fig. 4 in Conroy & Wechsler 2009). Assuming that a halo is on the mean M_*/M_{halo} relation at the time its star formation is quenched, Fig. 14 shows how far off the mean M_*/M_{halo} relation at $z = 0$ that halo would be as a function of the redshift of quenching. The details of this calculation are as follows: first, we set up the M_*/M_{halo} ratio as a function of halo mass through Eq. (1), using the halo plus subhalo mass function in Eq. (2). For stellar mass, we use the Li & White (2009) stellar mass function at $z = 0$, and we linearly interpolate to higher redshift stellar mass functions as given in Marchesini et al. (2007). We consider two different $z = 0$ halo mass bins: $M_{\text{halo}} = 10^{12} h^{-1} M_\odot$ and $10^{11.5} h^{-1} M_\odot$. Using our N -body simulation, we track these halos back in time and determine their masses as a function of redshift, assigning them galaxy masses that lie on the M_*/M_{halo} relation at each redshift. Assuming a galaxy is quenched at redshift z , we calculate the difference between the stellar mass at z and the mean relation at $z = 0$ for each halo mass bin. The earlier a galaxy is quenched, the larger the difference with respect to the typical galaxy mass for that halo mass. The currently best-estimated log-normal scatter in the M_*/M_{halo} relation at $z \sim 0$ is 0.15–0.2 dex (More et al. 2010; Leauthaud et al. 2011b), so the offset in Fig. 14 becomes larger than the scatter for centrals quenching prior to $z \approx 0.3$.

6 DISCUSSION

6.1 The Environmental Dependence of Galaxy Properties

In this paper we have demonstrated that the properties of galaxies at fixed halo mass are independent of density measured on scales larger than the halo radius, and that the dependence of the quenched fraction of galaxies on large-scale environment can be explained by the variations of the halo mass function with environment and by disentangling the relative contributions of central and satellite galaxies. Our results extends earlier works that demonstrated that galaxy properties correlate weakly with large-scale environment when small-scale environment is fixed on a 1 Mpc scale (Kauffmann et al. 2004; Blanton et al. 2006). However, we have argued that, because different galaxies live in different halos, it is not possible (or physically motivated) to find a single smoothing scale that fully determines galaxy properties at all masses. For rich groups and clusters, our results are in good agreement with Blanton & Berlind (2007), who found that the blue fraction of galaxies is independent of density at fixed group luminosity, though we do see evidence for some change with density for the brightest central galaxies. These results are in good agreement with the results of Peng et al. (2011), who also find that the environmental dependence of the red fraction of galaxies is driven primarily by satellite galaxies and not by centrals. In detail, the observations diverge from this scenario for quenched bright central galaxies and in the mean stellar ages of central galaxies on the star-forming sequence. But our results support the notion that halo mass is the dominant quantity governing the properties of the galaxies contained within them.

6.2 Halo Assembly Bias and the f_Q -Density Relation

As discussed in §1, the formation histories of dark matter halos depend on environment. For low-mass halos, old halos form in high-density environments. For high-mass halos, old halos form in low-density environments, although there is some debate on the amplitude of this correlation. If halo and galaxy formation histories are correlated, then our measurements are inconsistent with both of these theoretical results. Figs. 7 and 11 clearly demonstrate a lack of correlation between f_Q and $\rho/\bar{\rho}$ for low-mass galaxies. Fig. 13 demonstrates that the mean stellar ages of quenched central galaxies also is constant with $\rho/\bar{\rho}$. For galaxies below the knee is the stellar mass function, the ansatz that old galaxies live in old halos is not supported by the data.

However, the quenched fraction of central galaxies in $M_{\text{host}} \sim 10^{12.3} h^{-1} M_\odot$ halos show a positive correlation with environment. This is the mass scale at which halos in simulations show little-to-no correlation between age and $\rho/\bar{\rho}$. One possibility is that the environmental dependence for high-mass central galaxies arises from those that have passed through the virial radius of a more massive halo (and therefore reside higher density environments) but are counted as centrals at the present time (Gill et al. 2005; Ludlow et al. 2009; Wang et al. 2009). However, these ejected satellites are expected to become less common at increasing galaxy mass, so the effect is opposite to the trend we see here (we will discuss these processes in more detail in Papers II and III). Another possibility is that our assumption that the central galaxy is the most massive galaxy is becoming less valid at higher galaxy mass, as suggested by Skibba et al. (2011), and we are confusing high-mass centrals and satellites. However, in order to masquerade as the signal in Fig. 10, this effect would have to have strong environmental dependence, which remains unclear. Additionally, at higher halo masses, central and satellite galaxies have increasingly similar quenched fractions. Thus, the stellar mass dependences of Skibba et al. (2011) and central/satellite quenched fractions should cancel out at some level.

Our results have mixed agreement with those of Wang et al. (2008), who used a similar group-finding algorithm. They found that galaxy groups with redder overall colors have higher clustering than groups of the same mass but with bluer galaxies, in agreement with our results. However, they also found that the effect is stronger in less massive groups, opposite to the mass dependence we see here. Wang et. al. use color as a proxy for age as opposed to (dust-insensitive) D_n4000 , though it is unclear why using color would lead to a stronger signal.

6.3 The Stellar to Halo Mass Ratios of Low-Mass Galaxies

Galaxies that are star forming and galaxies that are quenched form in halos that growth the same average rate. This implies that the stellar mass to halo mass ratio, M_*/M_{halo} will evolve differently for quenched and star-forming galaxies. Fig. 14 demonstrates a $M_{\text{halo}} = 10^{11.5} h^{-1} M_\odot$ halo that contains a central galaxy quenched at $z = 0.6$ will have a M_*/M_{halo} ratio lower by a factor of

2.5 at $z = 0$ relative to the mean mean for that halo mass. However, weak lensing and satellite kinematical measurements of the halos masses of low-mass galaxies find that the halo masses are the same within the errors, regardless of color selection (Mandelbaum et al. 2006; More et al. 2010). This is in conflict with the conclusion that galaxy growth and halo growth are uncorrelated. There are several possible resolutions to this discrepancy.

(i) The observations of halo masses of low-mass central galaxies are biased due the use of color rather than D_n4000 for sample segregation. The low-mass red samples will contain many intrinsically star-forming galaxies, thus bringing the mean halo masses closer together. Lack of significant numbers also increase observational errors and low masses.

(ii) Low-mass galaxies on the red sequence were quenched recently, and thus have not had enough time to create a significant difference in the M_*/M_{halo} ratio. There is a clear red sequence at $z = 1$, but the fraction of quenched central galaxies at $M_* \lesssim 10^{10}$ is not known.

(iii) Sub- L_* central galaxies do not follow a one-way path to the red sequence; galaxies migrate back and forth from the blue cloud to the red sequence before permanently becoming quenched. Some blue galaxies at $z = 0$ may have been temporarily quenched previously, while some $z = 1$ red galaxies may still grow through star formation later. This would minimize the difference between the halo masses of red and blue central galaxies at fixed M_* .

Galaxies that are quenched, for example, by AGN heating or major galaxy mergers (e.g., Croton et al. 2006; Bower et al. 2006; Hopkins et al. 2008; Somerville et al. 2008) could still accrete gas or merge with gas-rich objects at some later time, replenishing their fuel supply and moving them back into the star-forming sequence. In hydrodynamical simulations of galaxy formation, low-mass halos ($M_{\text{halo}} \lesssim 10^{12} h^{-1} M_\odot$) accrete their gas in a cold state (Kereš et al. 2005; Dekel & Birnboim 2006; Kereš et al. 2009; Brooks et al. 2009). Thus previous merging or AGN activity that might temporarily quench a galaxy will not prevent any new gas from migrating to the center of the potential well within a dynamical time, even if the stellar population is old. However, none of these solutions are mutually exclusive, and it is possible that a all three cause the measurements presented here.

6.4 What Quenches Low-mass Central Galaxies?

The fraction of quenched central galaxies in the deepest voids is the same as that in regions around clusters. Thus the mechanism by which low-mass central galaxies stop their star-formation must be environmentally independent. Wang et al. (2009) note that many red dwarf galaxies are isolated, but propose that the majority of quenched central galaxies of this type are ejected satellites, low-mass halos that have passed through a group or cluster. The uniformity of f_Q^{cen} for low-mass galaxies argues strongly against such a model due to the strong environmental dependence that would result from such a model. We cannot rule out two mechanisms that operate primarily at low and high density, respectively, that add to a constant f_Q^{cen} , but Occam's razor argues against such a scenario.

We find that the Sersic indices of these galaxies does

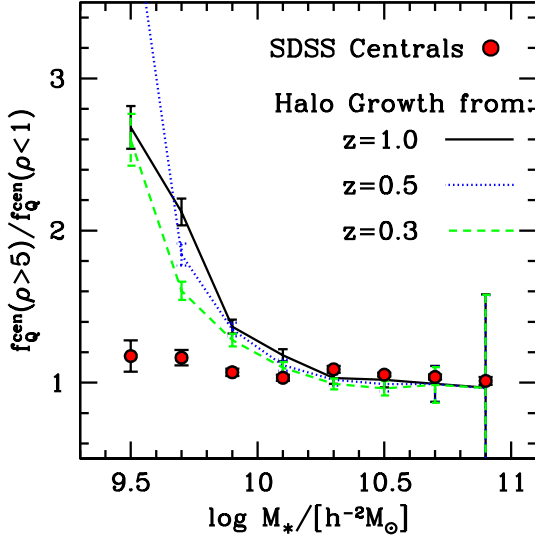


Figure 12. The ratio of the central quenched fraction between high- and low-density environments as a function of stellar mass. Filled circles show results from the group catalog, while curves indicate results using the growth rates of corresponding dark matter halos as measured over different redshift baselines.

not vary with density, with $\langle n_s \rangle \approx 3.5$. This implies that the mechanism that quenches low-mass centrals also induces morphological transformation. It also strengthens the claim that the process that halts star formation in centrals at high densities also operates at low densities.

Using semi-analytic models, Croton & Farrar (2008) find a small population of central galaxies quenched by AGN heating, but this process can only effect high-mass halos of $M_{\text{halo}} > 10^{12.5} h^{-1} M_{\odot}$, roughly an order or magnitude more massive than the host halos of the galaxies probed here, and even more massive than the dwarf galaxies in Wang et al. (2009).

Halo mergers vary only weakly with large-scale dark matter density (Fakhouri & Ma 2009), implying that the galaxy merger rate would also show no environmental dependence. Major mergers are also likely to cause a transition from disk-dominated to spheroidal-dominated morphology (see, e.g., Hopkins et al. 2008). But it remains unclear whether there are enough mergers to fully account for these objects. We leave this to a future study (Wetzel et. al., in preparation).

Further analysis of the morphologies and other properties of these galaxies, as well as their redshift evolution, will shed light on the mechanisms by which quenching occurs in these systems, and whether or not quenching is transient.

The authors would like to thank Frank van den Bosch for supplying the Yang et. al. group catalog, as well as useful discussions on the results presented in this paper.

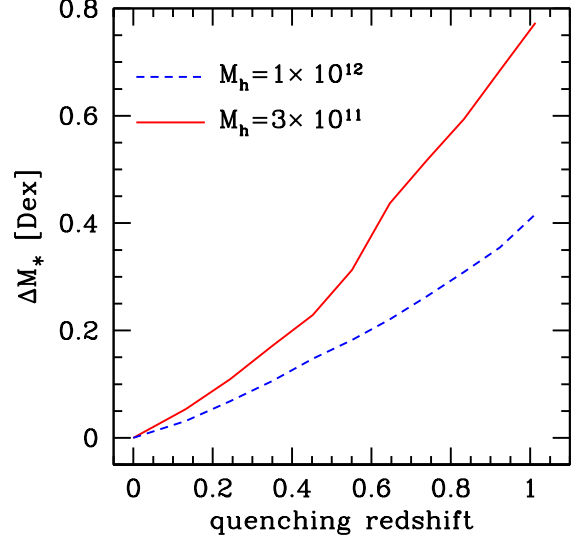


Figure 14. The difference in logarithmic stellar mass between the $z = 0$ mean M_* - M_{halo} relation and the relation for galaxies that were quenched at redshift z , as a function of z . This plot assumes that halo growth and galaxy growth are uncorrelated, thus when a galaxy is quenched the halo it resides in continues to grow at the mean rate up to $z = 0$. Solid and dashed curves are for halos with $z = 0$ masses of 3×10^{11} and $10^{12} h^{-1} M_{\odot}$, which host central galaxies of $\log M_* = 9.7$ and $10.2 h^{-1} M_{\odot}$, respectively.

APPENDIX A: REAL VS. REDSHIFT-SPACE DENSITY MEASURES

Here we test the correlation between large-scale galaxy density measured in real and redshift space. We use the numerical simulation of Wetzel & White (2010) in which dark matter (sub)halos are matched with galaxy luminosity by the abundance-matching method described in §2, and the subhalos are populated into a larger volume simulation as described in Tinker & Wetzel (2010). The volume of the simulation is $720^3 (h^{-1} \text{Mpc})^3$, larger than the $M_r < -20$ volume limited sample from Table 1. For each galaxy in the simulation, we determine the galaxy density in $10 h^{-1} \text{Mpc}$ spheres in both real space and redshift space, assuming the distant observer approximation thus using the z -axis of the simulation as the line of sight. Fig. A1 shows the correlation and scatter between the two. At this scale, the mean redshift-space density faithfully tracks the real-space density. More importantly, the scatter is generally $\lesssim 0.1$ dex within the extremes of the density field.

APPENDIX B: GROUP FINDING ALGORITHM

Here we describe our galaxy group finding algorithm in more detail. We define dark matter such that the mean density Δ interior to a radius R_{Δ} is 200 times the universal matter density $\bar{\rho} = \Omega_m \times \rho_{\text{crit}}$. Here and throughout this paper, R_{Δ} is in comoving units. Thus the mass and radius of a halo are related by

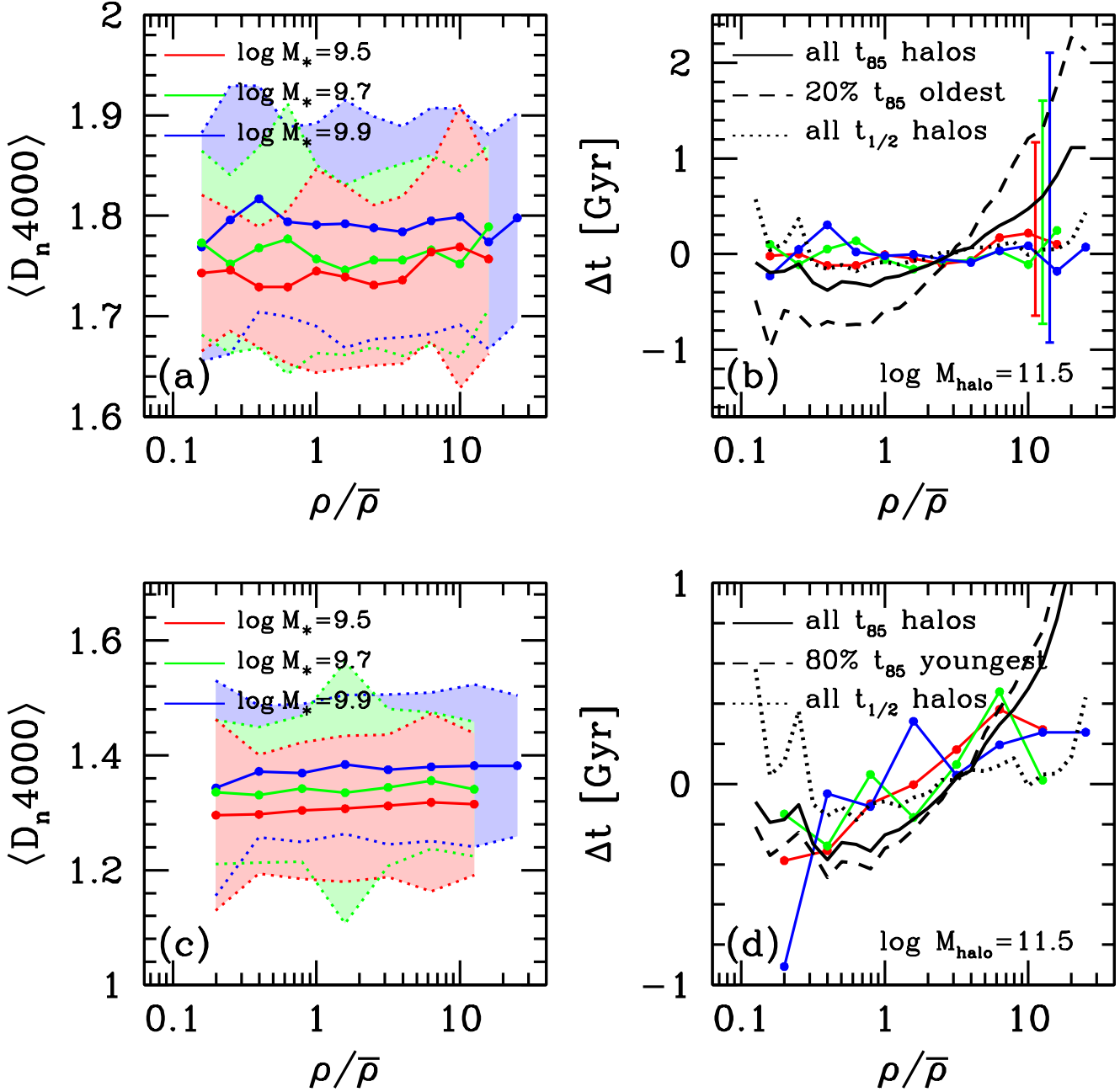


Figure 13. Panel (a): D_n4000 values for quiescent central galaxies as a function of $\rho/\bar{\rho}$. The connected dots indicate the mean D_n4000 for different M_* bins. The shaded regions indicate the dispersion for each stellar mass bin. Panel (b): The change in the mean quenching timescale inferred from $\langle D_n4000 \rangle$ in panel (a). Timescales are calculated from stellar population synthesis models described in the text. Here we plot Δt rather than absolute age because it is less sensitive to model assumptions. Connected dots represent the same stellar mass bins as in (a). The errorbars indicate the dispersion in Δt implied by the variance in D_n4000 . Black curves represent results from dark matter halos: the solid black curve is the change in the mean formation time t_{85} for halos of mass $10^{11.5} h^{-1} M_\odot$ (equivalent to the halo mass for $M_* = 10^{9.7} M_\odot/h^2$ central galaxies). Dashed black curve shows Δt for the oldest 20% of halos at each density bin (equivalent to f_Q for central galaxies with $M_* = 10^{9.7} M_\odot/h^2$). The dotted curve shows Δt for halos based on $t_{1/2}$. Panel (c): same as (a), but now for star-forming central galaxies (defined as $D_n4000 < 1.6$). Panel (d): Same as (b) but again for star-forming galaxies. In this panel, the dashed curve indicates Δt for the 80% youngest halos at each density (corresponding to the fraction of star-forming central galaxies). Note the change in y -axis range.

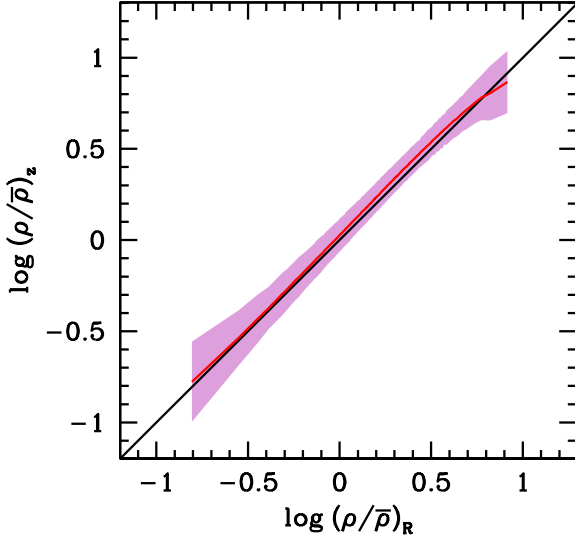


Figure A1. Comparison between galaxy density in redshift space and real space as measured in a sphere of radius $10 h^{-1}$ Mpc. Results are presented for mock galaxies within a $720^3 (h^{-1} \text{ Mpc})^{-3}$ simulation volume. The solid red curve shows the mean relation, and the shaded region shows the dispersion about the mean. The solid black curve shows where the two measures are equal.

$$M_{\Delta} = \frac{4}{3} \pi R_{\Delta}^3 \Delta \bar{\rho}. \quad (\text{B1})$$

In comoving units, $\bar{\rho}$ is a constant, thus the comoving radius of a halo is independent of redshift at fixed mass. Assuming the virial theorem, the velocity dispersion of the dark matter within a halo is

$$\sigma_v^2 = \frac{GM_{\Delta}}{2R_{\Delta}}(1+z), \quad (\text{B2})$$

where $G = 4.304 \times 10^{-9}$ in units of $(\text{km/s})^2 \text{Mpc}/\text{M}_{\odot}$, and the factor of $(1+z)$ is to convert the comoving radius to physics units.

Dark matter halos follow a ‘universal’ density profile described in Navarro et al. (1997a) (hereafter NFW), defined by a scale radius r_s and a concentration parameter $c_{\Delta} = R_{\Delta}/r_s$. The 2-D projected density profile of the NFW profile is given by

$$\Sigma(R) = 2 r_s \bar{\delta} \bar{\rho}_{\text{gal}} f(R/r_s), \quad (\text{B3})$$

with

$$f(x) = \begin{cases} \frac{1}{x^2-1} \left(1 - \frac{\ln \frac{1+\sqrt{1-x^2}}{x}}{\sqrt{1-x^2}} \right) & \text{if } x < 1 \\ \frac{1}{3} & \text{if } x = 1 \\ \frac{1}{x^2-1} \left(1 - \frac{\text{atan}\sqrt{x^2-1}}{\sqrt{x^2-1}} \right) & \text{if } x > 1 \end{cases}, \quad (\text{B4})$$

and

$$\bar{\delta} = \frac{200}{3} \frac{c_{200}^3}{\ln(1+c_{200}) - c_{200}/(1+c_{200})}, \quad (\text{B5})$$

where $\bar{\rho}_{\text{gal}}$ is the mean galaxy density in the volume-limited sample. Thus, in constructing galaxy groups, we assume that halos defined by a mean overdensity with respect to dark

matter of 200 will also appear at overdensities in the galaxy density field with $\Delta = 200$.

We assume that the velocity dispersion of satellite galaxies follows a Gaussian distribution with dispersion given in equation (B2). Thus the line-of-sight probability of a galaxy being a member of a group is defined by

$$p(\Delta v) = \frac{1}{\sqrt{2\pi}\sigma_v} \exp \left[\frac{-(\Delta v)^2}{2\sigma_v^2} \right], \quad (\text{B6})$$

where $\Delta v \equiv (z_{\text{gal}} - z_{\text{group}})/c$ and c is the speed of light, and the redshift of the group is defined as that of the central galaxy.

All together, the number density contrast of a group of galaxies over the background, as a function of both projected separation from the central galaxy R , and line-of-sight velocity difference from the central galaxy Δv , is expressed as

$$P(\Delta v, R) = \frac{c}{H_0} \frac{\Sigma(R)}{\bar{\rho}_{\text{gal}}} p(\Delta v). \quad (\text{B7})$$

For a given galaxy, if P is greater than a background value B , then the galaxy is considered to be a member of the group. We have calibrated $B = 0.5$ via our simulation mock catalog to maximize both completeness and purity. We proceed through the galaxy catalog in descending order of luminosity, and if a galaxy is classified as a satellite, it cannot be a central galaxy (by definition) and thus cannot have satellites of its own. In this algorithm, the brightest (or most massive) galaxy in a group is the central galaxy by definition.

Once galaxies have been assigned as centrals and satellites in dark matter halos, we recalculate halo mass. But we are now interested in deconvolving the galaxy distribution into the occupation of galaxies in host halos, we use the same abundance matching technique, but now we use the *total* group luminosity and match that with the host halo mass function (the Tinker et al. 2008 function). With the new halo masses, we go back to the beginning and re-classify galaxies as centrals and satellites, iterating the process until convergence.

APPENDIX C: TESTS OF THE GROUP FINDING ALGORITHM

The group finder described above has been thoroughly tested by Yang et al. (2005). Because we are using a slightly different implementation of the algorithm, and because we are probing density-dependent statistics that have not been explored in previous papers, we perform two additional checks on our group catalog.

C1 The Halo Occupation Distribution of the Group Catalog

The aim of the group finding algorithm is to associate every galaxy in the sample with a dark matter host halo, in the same framework as the halo occupation distribution (HOD). For a fixed cosmology, a given HOD maps uniquely onto a two-point correlation function. Thus a consistency check on the results of the group finder is to compare the observed correlation function of galaxies with that predicted by the HOD measured from the group sample.

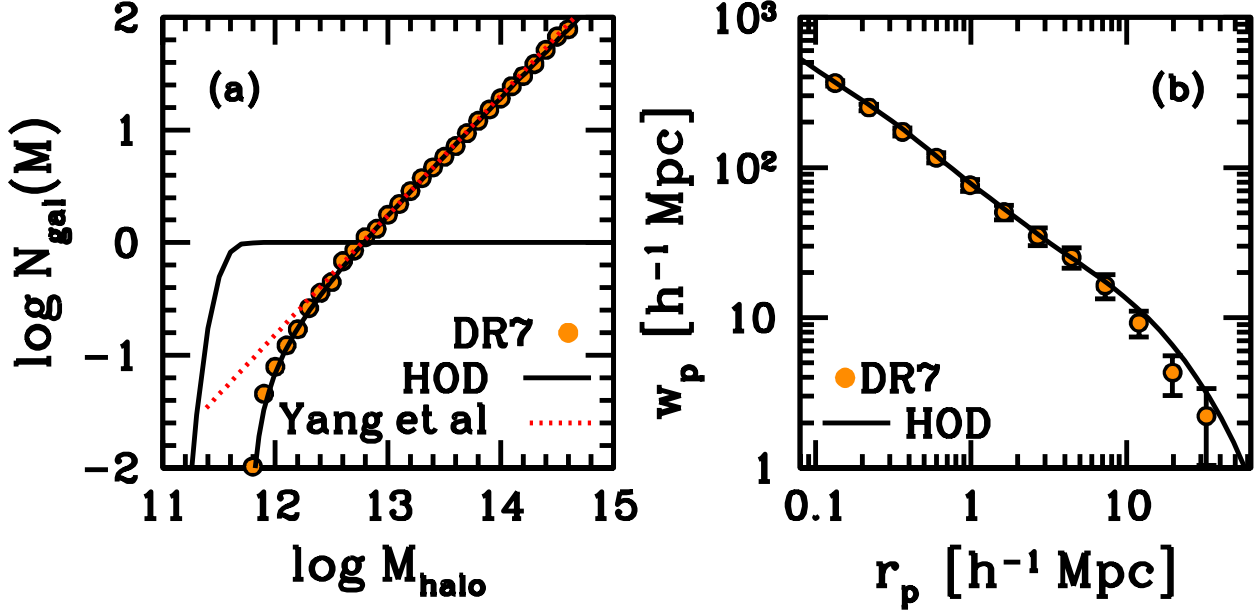


Figure B1. Panel (a): Circles represent the halo occupation of satellite galaxies with $M_r < -19$ as a function of halo mass as measured from the group catalog. The solid curve shows a parametric HOD fitted to these data; the curve that asymptotes to $\log N_{\text{gal}} = 0$ represents central galaxies. The dotted line is the power-law fit to N_{gal} for the same sample of galaxies from Yang et al. 2008 (their fit is restricted to $M_{\text{halo}} \gtrsim 12.3$). Panel (b): Points with errors represent measurements of the projected two-point correlation function, $w_p(r_p)$, from DR7 for $M_r < -19$ galaxies. The solid curve is the HOD prediction for $w_p(r_p)$ using the occupation function from panel (a).

Fig. B1a shows the the number of satellite galaxies with $M_r < -19$ as a function of host halo mass. The dotted curve shows the power-law fit to the same quantity from the Yang et al. (2008) SDSS DR4 results. They do not include results from $\langle N_{\text{sat}} \rangle_M < 0.1$ host halos in the fit. The black curves shows a fit to both $\langle N_{\text{sat}} \rangle_M$ and $\langle N_{\text{cen}} \rangle_M$ using the HOD parameterization in Tinker et al. (2008). Fig. B1b shows the measured projected two-point correlation function $w_p(r_p)$ from DR7. Here we have used the Landy & Szalay (1993) estimator for $w_p(r_p)$ and the random catalogs provided in the VAGC to account for the survey angular selection function. The black curve shows the predicted $w_p(r_p)$ from the HOD. We use the analytic model described in Tinker et al. (2005). The two correlation functions are in excellent agreement with one another, demonstrating the consistency of the halo occupation of the groups.

C2 Recovery of Galaxy Properties on Mocks

It is not possible to determine absolute membership of a group in redshift space. Group members may have large velocities relative to the group center, while non-members may be redshifted into the group from coherent infall. Thus, some fraction of the group members are not true members but are central galaxies that exist within a smaller halo. Alternately, some galaxies classified as low-mass centrals are actually members of a more massive group. (Satellites can also be misclassified across groups, but this is comparatively rare.) The test presented in Fig. B1 demonstrates that the *mean* number of members is not biased, but because satellite galaxies have different properties than central galaxies of the same magnitude, the mean properties of observed group

members will be biased. The true quenched fraction of satellite galaxies is higher than the true quenched fraction of centrals, thus the misclassification of central/satellite galaxies can *only* have the effect of reducing the observed f_Q^{sat} and increasing f_Q^{cen} .

To test our group finding algorithm, we apply it to a mock galaxy catalog from a $250 h^{-1} \text{Mpc}$ N -body simulation with a particle mass of $10^8 h^{-1} M_\odot$ and force resolution of $2.5 h^{-1} \text{kpc}$ (see White et al. 2010), which robustly resolves the subhalos that host galaxies we examine here. We describe the simulation, subhalo finding, and mock catalog generation in detail in Paper III. The cosmological parameters of this simulation are nearly identical to those assumed in this paper. Galaxy luminosities are assigned to halos and subhalos using the subhalo abundance matching technique described in §2. As defined in §1, galaxies within subhalos are labeled satellite galaxies, while all other galaxies are central. The positions of the galaxies are transformed from real space to redshift space using the distant observer approximation with the z -axis of the box being the line of sight.

The left panel in Fig. C1 shows purity and completeness of the groups determined via the mock. These statistics are broken down into central and satellite galaxies, plotted as a function of (intrinsic) host halo mass. Across most halo masses, the purity and completeness of central galaxies is over 90%. The purity and completeness of satellite galaxies is lower, $\sim 80\%$. The average overall fraction of galaxies that are misclassified—labeled as a central when they are intrinsically a satellite (or vice versa)—is 10%.

To test our recovery of the quenched fraction of galaxies, we randomly select 20% of all centrals to be quenched and we randomly select 80% of all satellite galaxies to be

quenched. These values were chosen to make the difference between central and satellite galaxies large in order to maximize any bias accrued by the group finder. The impurity and incompleteness of the group finding algorithm yields errors in the observed quenched fraction of central and satellite galaxies. The right panel in Fig. C1 shows the resulting values of f_Q as a function of density, similar to Fig. 7. The results of the group finder are shown with the circles with error bars. The observed f_Q^{sat} is reasonably accurate, but the observed f_Q^{cen} is biased low by more than 10%. At higher densities, the fraction of satellite galaxies increases, yielding a monotonically increasing f_Q^{cen} with $\rho/\bar{\rho}$.

If the fraction of misclassified galaxies is known, then this bias can be corrected for statistically. The number of quenched satellite galaxies is defined as

$$N_{\text{sat}} f_{Q,\text{obs}}^{(\text{sat})} = x f_Q^{\text{sat}} N_{\text{sat}} + (1 - y) f_Q^{\text{cen}} N_{\text{cen}}, \quad (\text{C1})$$

where x is the fraction of satellite galaxies correctly identified as satellites, and y is the fraction of centrals correctly identified as centrals. These two quantities are related by

$$(1 - x) N_{\text{sat}} = (1 - y) N_{\text{cen}}. \quad (\text{C2})$$

Equation (C1) reduces to

$$f_{Q,\text{obs}}^{(\text{sat})} = x f_Q^{\text{sat}} + (1 - x) f_Q^{\text{cen}}, \quad (\text{C3})$$

and the observed quenched fraction for centrals can be similarly written as

$$f_{Q,\text{obs}}^{(\text{cen})} = (1 - y) f_Q^{\text{sat}} + y f_Q^{\text{cen}}. \quad (\text{C4})$$

Solving equation (C4) for f_Q^{cen} and substituting into equation (C3), the intrinsic f_Q^{sat} is given by

$$f_Q^{\text{sat}} = \frac{y f_{Q,\text{obs}}^{(\text{sat})} + (x - 1) f_{Q,\text{obs}}^{(\text{cen})}}{xy + (x - 1)(1 - y)}. \quad (\text{C5})$$

Substitution of f_Q^{sat} back into equation (C4) yields the equation for f_Q^{cen} . We find that $x \approx 0.8$ in our N -body simulations (see Fig. C1, left panel), nearly independent of halo mass and large-scale density. To determine the overall quenched fraction of centrals, the misclassified fraction of centrals is $y \approx 0.8 N_{\text{sat}} / N_{\text{cen}} = 0.93$. To determine the f_Q^{cen} as a function of density, y is calculated at each value of $\rho/\bar{\rho}$. In practice, this procedure overcorrects for f_Q^{cen} at the densities where $N_{\text{sat}} > N_{\text{cen}}$ (roughly $\rho/\bar{\rho} \gtrsim 6$, or the rightmost 2 data points in Fig. C1). In this regime, we fix $y = 0.85$ and calculate x through equation (C2).

The solid curves in right panel of Fig. C1 show the results of applying the above procedure to the measured values of $f_{Q,\text{obs}}^{(\text{cen})}$ and $f_{Q,\text{obs}}^{(\text{sat})}$.

REFERENCES

Abazajian K. N., et al., 2009, ApJS, 182, 543
 Abbas U., Sheth R. K., 2006, MNRAS, 372, 1749
 Baldry I. K., Balogh M. L., Bower R. G., Glazebrook K., Nichol R. C., Bamford S. P., Budavari T., 2006, MNRAS, 373, 469
 Balogh M., Eke V., Miller C., Lewis I., Bower R., Couch W., Nichol R., Bland-Hawthorn J., Baldry I. K., Baugh C., Bridges T., Cannon R., Cole S., Colless M., Collins

C., Cross N., Dalton G., de Propris R., Driver S. P., Efstathiou G., Ellis R. S., Frenk C. S., Glazebrook K., Gomez P., Gray A., Hawkins E., Jackson C., Lahav O., Lumsden S., Maddox S., Madgwick D., Norberg P., Peacock J. A., Percival W., Peterson B. A., Sutherland W., Taylor K., 2004, MNRAS, 348, 1355
 Bamford S. P., Nichol R. C., Baldry I. K., Land K., Lintott C. J., Schawinski K., Slosar A., Szalay A. S., Thomas D., Torki M., Andreescu D., Edmondson E. M., Miller C. J., Murray P., Raddick M. J., Vandenberg J., 2009, MNRAS, 393, 1324
 Behroozi P. S., Conroy C., Wechsler R. H., 2010, ApJ, 717, 379
 Bell E. F., Wolf C., Meisenheimer K., Rix H.-W., Borch A., Dye S., Kleinheinrich M., Wisotzki L., McIntosh D. H., 2004, ApJ, 608, 752
 Berlind A. A., Frieman J., Weinberg D. H., Blanton M. R., Warren M. S., Abazajian K., Scranton R., Hogg D. W., Scoccimarro R., Bahcall N. A., Brinkmann J., Gott III J. R., Kleinman S. J., Krzesinski J., Lee B. C., Miller C. J., Nitta A., Schneider D. P., Tucker D. L., Zehavi I., 2006, ApJS, 167, 1
 Berlind A. A., Weinberg D. H., 2002, ApJ, 575, 587
 Blanton M. R., Berlind A. A., 2007, ApJ, 664, 791
 Blanton M. R., Eisenstein D., Hogg D. W., Schlegel D. J., Brinkmann J., 2005, ApJ, 629, 143
 Blanton M. R., Eisenstein D., Hogg D. W., Zehavi I., 2006, ApJ, 645, 977
 Blanton M. R., Hogg D. W., Bahcall N. A., Baldry I. K., Brinkmann J., Csabai I., Eisenstein D., Fukugita M., Gunn J. E., Ivezić Ž., Lamb D. Q., Lupton R. H., Loveday J., Munn J. A., Nichol R. C., Okamura S., Schlegel D. J., Shimasaku K., Strauss M. A., Vogeley M. S., Weinberg D. H., 2003, ApJ, 594, 186
 Blanton M. R., Hogg D. W., Bahcall N. A., Brinkmann J., Britton M., Connolly A. J., Csabai I., Fukugita M., Loveday J., Meiksin A., Munn J. A., Nichol R. C., Okamura S., Quinn T., Schneider D. P., Shimasaku K., Strauss M. A., Tegmark M., Vogeley M. S., Weinberg D. H., 2003, ApJ, 592, 819
 Blanton M. R., Roweis S., 2007, AJ, 133, 734
 Blanton M. R., Schlegel D. J., Strauss M. A., Brinkmann J., Finkbeiner D., Fukugita M., Gunn J. E., Hogg D. W., Ivezić Ž., Knapp G. R., Lupton R. H., Munn J. A., Schneider D. P., Tegmark M., Zehavi I., 2005, AJ, 129, 2562
 Bond J. R., Cole S., Efstathiou G., Kaiser N., 1991, ApJ, 379, 440
 Bower R. G., Benson A. J., Malbon R., Helly J. C., Frenk C. S., Baugh C. M., Cole S., Lacey C. G., 2006, MNRAS, 370, 645
 Brinchmann J., Charlot S., White S. D. M., Tremonti C., Kauffmann G., Heckman T., Brinkmann J., 2004, MNRAS, 351, 1151
 Brooks A. M., Governato F., Quinn T., Brook C. B., Wadsley J., 2009, ApJ, 694, 396
 Chabrier G., 2003, PASP, 115, 763
 Conroy C., Gunn J. E., White M., 2009, ApJ, 699, 486
 Conroy C., Gunn J. E., 2010, ApJ, 712, 833
 Conroy C., Wechsler R. H., 2009, ApJ, 696, 620
 Conroy C., Wechsler R. H., Kravtsov A. V., 2006, ApJ, 647, 201
 Cooper M. C., Newman J. A., Madgwick D. S., Gerke B. F.,

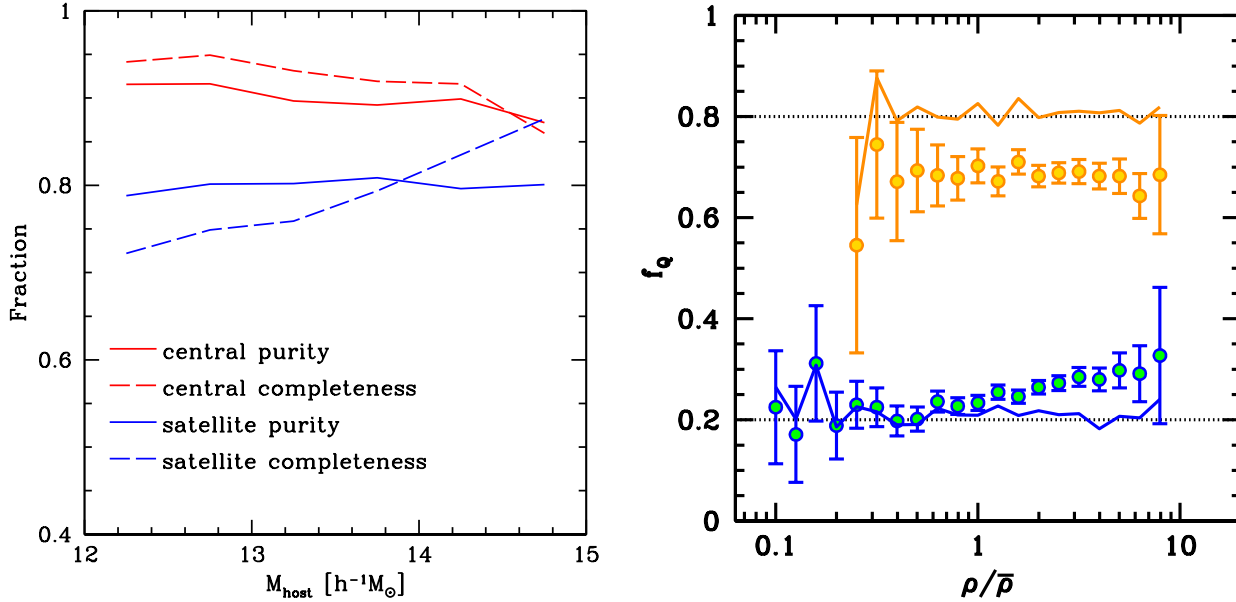


Figure C1. *Left panel:* The purity and completeness of the group finder vs. halo mass for all galaxies with $M_r < -19$, determined from applying the group finder to a mock galaxy distribution from simulation. Purity is defined by the fraction of centrals/satellites in the group finder that were of the same type in the input catalog, while completeness is defined by the fraction of centrals/satellites in the input distribution that were assigned to the same type by the group finder. *Right panel:* Quenched fractions for central and satellite galaxies vs. $10 h^{-1}$ Mpc overdensity. Dotted lines show the input values, circles show the measurements from the group finder, and solid curves show the corrected values from equations (C5) and (C3).

Yan R., Davis M., 2005, *ApJ*, 634, 833

Cooper M. C., Newman J. A., Coil A. L., Croton D. J., Gerke B. F., Yan R., Davis M., Faber S. M., Guhathakurta P., Koo D. C., Weiner B. J., Willmer C. N. A., 2007, *MNRAS*, 376, 1445

Cooper M. C., Newman J. A., Croton D. J., Weiner B. J., Willmer C. N. A., Gerke B. F., Madgwick D. S., Faber S. M., Davis M., Coil A. L., Finkbeiner D. P., Guhathakurta P., Koo D. C., 2006, *MNRAS*, 370, 198

Cooray A., Sheth R., 2002, *Phys. Rep.*, 372, 1

Croton D. J., Farrar G. R., 2008, *MNRAS*, 386, 2285

Croton D. J., Gao L., White S. D. M., 2007, *MNRAS*, 374, 1303

Croton D. J., Springel V., White S. D. M., De Lucia G., Frenk C. S., Gao L., Jenkins A., Kauffmann G., Navarro J. F., Yoshida N., 2006, *MNRAS*, 365, 11

Cucciati O., et al., 2006, *A&A*, 458, 39

Dalal N., White M., Bond J. R., Shirokov A., 2008, *ApJ*, 687, 12

Davis M., Geller M. J., 1976, *ApJ*, 208, 13

Dekel A., Birnboim Y., 2006, *MNRAS*, 368, 2

Dressler A., 1980, *ApJ*, 236, 351

Drory N., Bundy K., Leauthaud A., Scoville N., Capak P., Ilbert O., Kartaltepe J. S., Kneib J. P., McCracken H. J., Salvato M., Sanders D. B., Thompson D., Willott C. J., 2009, *ApJ*, 707, 1595

Fakhouri O., Ma C.-P., 2009, *MNRAS*, 394, 1825

Gao L., Springel V., White S. D. M., 2005, *MNRAS*, 363, L66

Gao L., White S. D. M., 2006

Gill S. P. D., Kneib A., Gibson B. K., 2005, *MNRAS*, 356, 1327

Haas M. R., Schaye J., Jeason-Daniel A., 2011, *MNRAS*,

submitted, ArXiv:1103.0547

Hansen S. M., Sheldon E. S., Wechsler R. H., Koester B. P., 2009, *ApJ*, 699, 1333

Harker G., Cole S., Helly J., Frenk C., Jenkins A., 2006, *MNRAS*, 367, 1039

Hogg D. W., Blanton M. R., Brinchmann J., Eisenstein D. J., Schlegel D. J., Gunn J. E., McKay T. A., Rix H., Bahcall N. A., Brinkmann J., Meiksin A., 2004, *ApJ*, 601, L29

Hopkins P. F., Cox T. J., Kereš D., Hernquist L., 2008, *ApJS*, 175, 390

Kauffmann G., Heckman T. M., White S. D. M., Charlot S., Tremonti C., Peng E. W., Seibert M., Brinkmann J., Nichol R. C., SubbaRao M., York D., 2003, *MNRAS*, 341, 54

Kauffmann G., White S. D. M., Heckman T. M., Ménard B., Brinchmann J., Charlot S., Tremonti C., Brinkmann J., 2004, *MNRAS*, 353, 713

Kereš D., Katz N., Fardal M., Davé R., Weinberg D. H., 2009, *MNRAS*, 395, 160

Kereš D., Katz N., Weinberg D. H., Davé R., 2005, *MNRAS*, 363, 2

Kimm T., Somerville R. S., Yi S. K., van den Bosch F. C., Salim S., Fontanot F., Monaco P., Mo H., Pasquali A., Rich R. M., Yang X., 2009, *MNRAS*, 394, 1131

Kravtsov A. V., Berlind A. A., Wechsler R. H., Klypin A. A., Gottlöber S., Allgood B., Primack J. R., 2004, *ApJ*, 609, 35

Landy S. D., Szalay A. S., 1993, *ApJ*, 412, 64

Leauthaud A., Tinker J., Behroozi P. S., Busha M. T., Wechsler R., 2011, ArXiv:1103.2077

Leauthaud A., Tinker J., Bundy K., Behroozi P. S., Massey R., Rhodes J., George M. R., Kneib J.-P., Benson A.,

- Wechsler R. H., Busha M. T., Capak P., Cortes M., Ilbert O., Koekemoer A. M., Le Fevre O., Lilly S., McCracken H. J., Salvato M., Schrabback T., Scoville N., Smith T., Taylor J. E., 2011b, ArXiv:1104.0928
- Li C., Kauffmann G., Jing Y. P., White S. D. M., Börner G., Cheng F. Z., 2006, MNRAS, 368, 21
- Li C., White S. D. M., 2009, MNRAS, 398, 2177
- Li Y., Mo H. J., Gao L., 2008, MNRAS, 389, 1419
- Lintott C., Schawinski K., Bamford S., Slosar A., Land K., Thomas D., Edmondson E., Masters K., Nichol R. C., Raddick M. J., Szalay A., Andreescu D., Murray P., Vandenberg J., 2011, MNRAS, 410, 166
- Ludlow A. D., Navarro J. F., Springel V., Jenkins A., Frenk C. S., Helmi A., 2009, ApJ, 692, 931
- Macciò A. V., Dutton A. A., van den Bosch F. C., 2008, MNRAS, 391, 1940
- Madgwick D. S., Somerville R., Lahav O., Ellis R., 2003, MNRAS, 343, 871
- Maller A. H., 2008, in Funes J. G., Corsini E. M., eds, *Astronomical Society of the Pacific Conference Series Vol. 396 of Astronomical Society of the Pacific Conference Series, Halo Mergers, Galaxy Mergers, and Why Hubble Type Depends on Mass*. pp 251–+
- Maller A. H., Berlind A. A., Blanton M. R., Hogg D. W., 2009, ApJ, 691, 394
- Mandelbaum R., Seljak U., Kauffmann G., Hirata C. M., Brinkmann J., 2006, MNRAS, 368, 715
- Marchesini D., van Dokkum P., Quadri R., Rudnick G., Franx M., Lira P., Wuyts S., Gawiser E., Christlein D., Toft S., 2007, ApJ, 656, 42
- Masters K. L., Mosleh M., Romer A. K., Nichol R. C., Bamford S. P., Schawinski K., Lintott C. J., Andreescu D., Campbell H. C., Crowcroft B., Doyle I., Edmondson E. M., Murray P., Raddick M. J., Slosar A., Szalay A. S., Vandenberg J., 2010, MNRAS, 405, 783
- Masters K. L., Nichol R., Bamford S., Mosleh M., Lintott C. J., Andreescu D., Edmondson E. M., Keel W. C., Murray P., Raddick M. J., Schawinski K., Slosar A., Szalay A. S., Thomas D., Vandenberg J., 2010, MNRAS, 404, 792
- More S., van den Bosch F. C., Cacciato M., Skibba R., Mo H. J., Yang X., 2010, MNRAS, in press, (arXiv:1003.3203), pp 1464–+
- Moster B. P., Somerville R. S., Maubetsch C., van den Bosch F. C., Macciò A. V., Naab T., Oser L., 2010, ApJ, 710, 903
- Navarro J. F., Frenk C. S., White S. D. M., 1997a, ApJ, 490, 493
- Navarro J. F., Frenk C. S., White S. D. M., 1997b, ApJ, 490, 493
- Noeske K. G., Faber S. M., Weiner B. J., Koo D. C., Primack J. R., Dekel A., Papovich C., Conselice C. J., Le Floch E., Rieke G. H., Coil A. L., Lotz J. M., Somerville R. S., Bundy K., 2007, ApJ, 660, L47
- Norberg P., Baugh C. M., Hawkins E., Maddox S., Madgwick D., Lahav O., Cole S., Frenk C. S., Baldry I., Bland-Hawthorn J., Bridges T., Cannon R., Colless M., Collins C., Couch W., Dalton G., De Propriis R., Driver S. P., Efsthathiou G., Ellis R. S., Glazebrook K., Jackson C., Lewis I., Lumsden S., Peacock J. A., Peterson B. A., Sutherland W., Taylor K., 2002, MNRAS, 332, 827
- Norberg P., Baugh C. M., Hawkins E., Maddox S., Peacock J. A., Cole S., Frenk C. S., Bland-Hawthorn J., Bridges T., Cannon R., Colless M., Collins C., Couch W., Dalton G., De Propriis R., Driver S. P., Efsthathiou G., Ellis R. S., Glazebrook K., Jackson C., Lewis I., Lumsden S., Peacock J. A., Peterson B. A., Sutherland W., Taylor K., 2002, MNRAS, 332, 827
- Oemler Jr. A., 1974, ApJ, 194, 1
- Park C., Choi Y.-Y., Vogeley M. S., Gott J. R. I., Blanton M. R., 2007, ApJ, 658, 898
- Peacock J. A., Smith R. E., 2000, MNRAS, 318, 1144
- Peng Y., Lilly S. J., Renzini A., Carollo M., 2011, ArXiv:1106.2546
- Scoccimarro R., Sheth R. K., Hui L., Jain B., 2001, ApJ, 546, 20
- Seljak U., 2000, MNRAS, 318, 203
- Sheth R. K., Tormen G., 2002, MNRAS, 329, 61
- Skibba R., Sheth R. K., Connolly A. J., Scranton R., 2006, MNRAS, 369, 68
- Skibba R. A., van den Bosch F. C., Yang X., More S., Mo H., Fontanot F., 2011, MNRAS, 410, 417
- Somerville R. S., Hopkins P. F., Cox T. J., Robertson B. E., Hernquist L., 2008, MNRAS, pp 1241–+
- Strateva I., Ivezić Ž., Knapp G. R., Narayanan V. K., Strauss M. A., Gunn J. E., Lupton R. H., Schlegel D., Bahcall N. A., Brinkmann J., Brunner R. J., Budavári T., Csabai I., Castander F. J., Doi M., Fukugita M., Györy Z., Hamabe M., Hennessy G., Ichikawa T., Kunszt P. Z., Lamb D. Q., McKay T. A., Okamura S., Racusin J., Sekiguchi M., Schneider D. P., Shimasaku K., York D., 2001, AJ, 122, 1861
- Swanson M. E. C., Tegmark M., Blanton M., Zehavi I., 2008, MNRAS, 385, 1635
- Swanson M. E. C., Tegmark M., Hamilton A. J. S., Hill J. C., 2008, MNRAS, 387, 1391
- Tinker J., Kravtsov A. V., Klypin A., Abazajian K., Warren M., Yepes G., Gottlöber S., Holz D. E., 2008, ApJ, 688, 709
- Tinker J. L., Conroy C., Norberg P., Patiri S. G., Weinberg D. H., Warren M. S., 2008, ApJ, 686, 53
- Tinker J. L., Weinberg D. H., Zheng Z., Zehavi I., 2005, ApJ, 631, 41
- Tinker J. L., Wetzel A. R., 2010, ApJ, 719, 88
- Vale A., Ostriker J. P., 2006, MNRAS, 371, 1173
- van den Bosch F. C., Aquino D., Yang X., Mo H. J., Pasquali A., McIntosh D. H., Weinmann S. M., Kang X., 2008, MNRAS, 387, 79
- van den Bosch F. C., Pasquali A., Yang X., Mo H. J., Weinmann S., McIntosh D. H., Aquino D., 2008, MNRAS, submitted, ArXiv:0805.0002
- van der Linden A., Wild V., Kauffmann G., White S. D. M., Weinmann S., 2010, MNRAS, 404, 1231
- Wang L., Li C., Kauffmann G., De Lucia G., 2006, MNRAS, 371, 537
- Wang Y., Yang X., Mo H. J., van den Bosch F. C., Weinmann S. M., Chu Y., 2008, ApJ, 687, 919
- Wang H., Mo H. J., Jing Y. P., 2009, MNRAS, 396, 2249
- Wang Y., Yang X., Mo H. J., van den Bosch F. C., Katz N., Pasquali A., McIntosh D. H., Weinmann S. M., 2009, ApJ, 697, 247
- Wechsler R. H., Zentner A. R., Bullock J. S., Kravtsov A. V., Allgood B., 2006, ApJ, 652, 71
- Weinmann S. M., van den Bosch F. C., Yang X., Mo H. J.,

- 2006, MNRAS, 366, 2
- Weinmann S. M., van den Bosch F. C., Yang X., Mo H. J., Croton D. J., Moore B., 2006, MNRAS, 372, 1161
- Weinmann S. M., Kauffmann G., von der Linden A., De Lucia G., 2010, MNRAS, 406, 2249
- Wetzel A. R., Cohn J. D., White M., Holz D. E., Warren M. S., 2007, ApJ, 656, 139
- Wetzel A. R., White M., 2010, MNRAS, 403, 1072
- White M., Cohn J. D., Smit R., 2010, MNRAS, 408, 1818
- Williams R. J., Quadri R. F., Franx M., van Dokkum P., Labbé I., 2009, ApJ, 691, 1879
- Willmer C. N. A., Faber S. M., Koo D. C., Weiner B. J., Newman J. A., Coil A. L., Connolly A. J., Conroy C., Cooper M. C., Davis M., Finkbeiner D. P., Gerke B. F., Guhathakurta P., Harker J., Kaiser N., Kassin S., Konidaris N. P., Lin L., Luppino G., Madgwick D. S., Noeske K. G., Phillips A. C., Yan R., 2006, ApJ, 647, 853
- Wilman D. J., Zibetti S., Budavári T., 2010, MNRAS, 406, 1701
- Yang X., Mo H. J., van den Bosch F. C., 2006, ApJ, 638, L55
- Yang X., Mo H. J., van den Bosch F. C., 2008, ApJ, 676, 248
- Yang X., Mo H. J., van den Bosch F. C., 2009, ApJ, 695, 900
- Yang X., Mo H. J., van den Bosch F. C., Jing Y. P., 2005, MNRAS, 356, 1293
- Yang X., Mo H. J., van den Bosch F. C., Pasquali A., Li C., Barden M., 2007, ApJ, 671, 153
- York D. G., et al., 2000, AJ, 120, 1579
- Zehavi I., Blanton M. R., Frieman J. A., Weinberg D. H., Mo H. J., Strauss M. A., et al., 2002, ApJ, 571, 172
- Zehavi I., Zheng Z., Weinberg D. H., Blanton M. R., Bahcall N. A., Berlind A. A., Brinkmann J., Frieman J. A., Gunn J. E., Lupton R. H., Nichol R. C., Percival W. J., Schneider D. P., Skibba R. A., Strauss M. A., Tegmark M., York D. G., 2010, ApJ, submitted (arXiv:1005.2413)
- Zehavi I., Zheng Z., Weinberg D. H., Frieman J. A., Berlind A. A., Blanton M. R., Scoccimarro R., Sheth R. K., Strauss M. A., Kayo I., Suto Y., Fukugita M., Nakamura O., Bahcall N. A., Brinkmann J., Gunn J. E., Hennessy G. S., Ivezić Ž., Knapp G. R., Loveday J., Meiksin A., Schlegel D. J., Schneider D. P., Szapudi I., Tegmark M., Vogeley M. S., York D. G., 2005, ApJ, 630, 1
- Zheng Z., Berlind A. A., Weinberg D. H., Benson A. J., Baugh C. M., Cole S., Davé R., Frenk C. S., Katz N., Lacey C. G., 2005, ApJ, 633, 791
- Zhu G., Zheng Z., Lin W. P., Jing Y. P., Kang X., Gao L., 2006, ApJ, 639, L5